



Geospatial Assessment of Hydrogeochemical Factors Controlling Groundwater Evolution of the Eocene Limestone and Clastic Quaternary Aquifers, Eastern Desert, Egypt

Hakeem Musaed · Ahmed Mosa · Gemail Khaled · Sayed Bedair · Thoria Zaky · Mohamed El Alfy

Received: 1 December 2023 / Accepted: 1 August 2024 / Published online: 14 August 2024
© The Author(s), under exclusive licence to Springer Nature Switzerland AG 2024

Abstract Hydrochemical studies, involving groundwater analysis, multivariate statistics, and geospatial element distributions, were carried out to understand the factors influencing groundwater geochemistry and potential pollution in an arid area (Eastern Desert, Egypt). A total of 104 groundwater samples were analyzed for twenty-three physical and chemical variables. Spatial mapping was conducted to depict variations in the concentration of several variables.

A spatial pattern revealed an increasing water table depth from south to north, correlating with a rise in groundwater salinity. The correlation coefficients for various variables were found to align with aquifer mineral saturation indices. Hydrochemical facies identified three main zones with six facies in the first sub-area, five in the second, and the third sub-areas. Specific processes, including evaporite/carbonate rock dissolution and ion exchange, dominate. The results support meteoric groundwater recharge in the first sub-area, influenced by the Nile water and rainfall. The second and third sub-areas indicated groundwater mixing from diverse sources, emphasizing evaporite/carbonate rock dissolution and ion exchange. Negative saturation indices for anhydrite, halite, and gypsum suggested under-saturation conditions, while dolomite and calcite indicated upper saturation, implying secondary mineral precipitation. Factor analysis demonstrated that six interrelated factors elucidate the chemical attributes of the groundwater. These factors arise from interactions between rock and water, blending of waters from diverse sources, and, to some extent, anthropogenic influences. Utilizing cluster analysis, notable and distinct groundwater zones were identified, where the original groundwater was uniquely influenced by mixing processes. Therefore, integration of hydrochemical and geospatial statistical analysis methods can be employed to enhance water resource management on a regional scale and in areas with similar conditions.

H. Musaed (✉) · M. E. Alfy
Geology Department, Faculty of Science, Mansoura University, Mansoura 35516, Egypt
e-mail: hakeem21112@gmail.com

H. Musaed
Department of Geological Engineering, Faculty of Oil and Minerals, University of Shabwah, Shabwah, Yemen

A. Mosa
Department of Soils, Faculty of Agriculture, Mansoura University, Mansoura 35516, Egypt

G. Khaled
Environmental Geophysics Lab (ZEGL), Geology Department, Faculty of Science, Zagazig University, Zagazig, Egypt

S. Bedair
The Research Institute for Groundwater (RIGW), Ministry of Water Resources & Irrigation, Kanater Khairia, Egypt

T. Zaky
Central Laboratory for Environmental Quality Monitoring (CLEQM), National Water Research Center (NWRC), Shubra Al Kheimah, Egypt

Keywords Rock-water interaction · Groundwater origin · Multivariate · Factor and cluster analyses

1 Introduction

Groundwater is a vital source of freshwater supply in arid and semi-arid regions to sustain agricultural, industrial and human consumption needs (El-Alfy et al., 2018). Among arid countries, Egypt reached the lowest per capita water shares in the world (approximately 550 m³ per capita per year) due to the high growth population (113 million in 2023) and the stable water budget from the Nile River (55.5 billion cubic meters annually), which represent about 97% of the total water demand (Abd Ellah, 2020). Furthermore, Egypt imports annually about 40 billion cubic meters of "virtual water" embedded in food imports to meet population needs (Ayyad & Khalifa, 2021). The most notable groundwater resources in Egypt include the Nile Valley and Delta aquifer, the Nubian Sandstone aquifer, Moghra, and the fractured limestone aquifer in the Eastern and western Deserts and Sinai Peninsula (El Alfy et al., 2019; Gemail et al., 2021; Ibrahim et al., 2023).

The Eastern Desert covers about 22% of the Egyptian territories, where groundwater represents an important resource and requires an effective assessment (Embaby et al., 2016). Groundwater of the Eastern Desert of Egypt is affected by several structural elements, which correlated with the Pan African Orogeny (e.g. fractures, folds, faults and shear zones) and subsequent tectonic reactivations, especially during Oligocene and Cretaceous times (Hussien, 2023). Groundwater resources in the Eastern Desert are scarce, and mainly occur in shallow alluvial and fracture zone aquifers, as well as sandstone and fractured carbonate aquifers (Abdel Moneim, 2005; Sultan et al., 2011). Direct recharge of these shallow alluvial and fracture zone aquifers occurs through seasonal rainfall and infrequent flash floods (Porsani et al., 2005; Ruelleu et al., 2010). The shallow alluvial and fracture zone aquifers can offer significant sources of groundwater at a local level, their utilization is restricted due to their relatively small frame and extensions and reliance on low precipitation recharge rates that occur over decades (Amer et al., 2012; Gemail et al., 2024).

Aquifer is not only a location for storing and transporting of groundwater, but also a domain for water rock interaction. In this regard, excessive release of fluoride in groundwater from different geogenic sources has been considered as a great challenge for groundwater utilization. In view of this, it is reported that 300 million people across Egypt and other arid countries 29 countries are suffering from endemic fluorosis, mainly because of the daily basis of F⁻ intake with groundwater for several human purposes (Sahoo et al., 2022). Besides, several anthropogenic activities might cause degradation and/or contamination of groundwater resource including mining, industrial sewage discharges (Gemail et al., 2017; Youssef et al., 2024), landfill sites and agricultural activities (Gemail et al., 2024; Zhai et al., 2022). For instance, a high degradation of water quality in groundwater of Gabes region, Tunisia was recorded due to the overuse of mineral fertilizers (Wederni et al., 2023). Another report showed elevated levels of arsenic, fluoride, and nitrate in the groundwater of southwestern part of New Mexico, USA (Islam, 2023). Consequently, there is an urgent need to monitor the quality of groundwater resources in arid regions for sustainable management of such limited water resources.

Overexploitation is also considered as one of the most important threats for the sustainable utilization of the groundwater aquifers in arid regions. As such, a tremendous decline by about 60m was recorded in the water level of Nubian aquifer in Egypt (El Alfy, 2013; Machiwal et al., 2018). The depletion of groundwater level is also linked with vulnerability of chemical contamination of the aquifer. For example, overexploitation of groundwater in Malwa region Punjab, India led to significant alterations in the aquifer chemistry (Kumar et al., 2023). In addition, the overuse of groundwater in Bastam region, Iran following alterations in precipitation regime (2002–2016) caused intrusion of saline water toward the aquifer due to the decline in groundwater level by about of 90 cm y⁻¹ and water storage deficit by about 17.32 Mm³ y⁻¹ (Bagheri et al., 2019).

The arid water storage basins have various hydrochemical environments and a zonal hydrogeochemical characters, this is due to various geological and metrological conditions (Li et al., 2019). Using of multivariate statistical methods is crucial in determining the natural processes that affect groundwater

and resolving hydrochemistry problems (Gulgundi & Shetty, 2018). Several studies had been carried out to assess groundwater potentialities (Ammar & Kamal, 2018; El-Ammawy et al., 2020; Gad & Saad, 2017; Khalil et al., 2021; H. Musaed et al., 2022). The current study is carried out in the area between south-east of Beni Suef and northeast El-Minia, Egypt. Which represents the eastern desert fringes of the Nile Valley. One hundred and four groundwater samples were collected and analyzed for major, minor and trace elements to evaluate the main hydrochemical processes that control the geochemistry of groundwater. The study area is divided into three main zones, depending on geological setting, lineament map and the water geochemistry. The main goal of the present study not only relies on the hydrochemical evaluation of groundwater, but also incorporates the utilization

of multivariate geostatistical technique to identify the major processes account for maximum variability in the analyzed data set such as; evaporation, mineral dissolution, precipitation, and anthropogenic factors.

2 Materials and Methods

2.1 Study Area

The study area located between south-east of Beni Suef and northeast El-Minia governorates, Egypt (longitudes of 30°48' – 31°5' E and latitudes of 28°18' – 28°52' N (Fig. 1). The studied area classified into three main zones. The elevation of first zones ranges from 9 m (asl) at the low-lying plain near the Nile River to 147 m (asl) at the southeastern part with

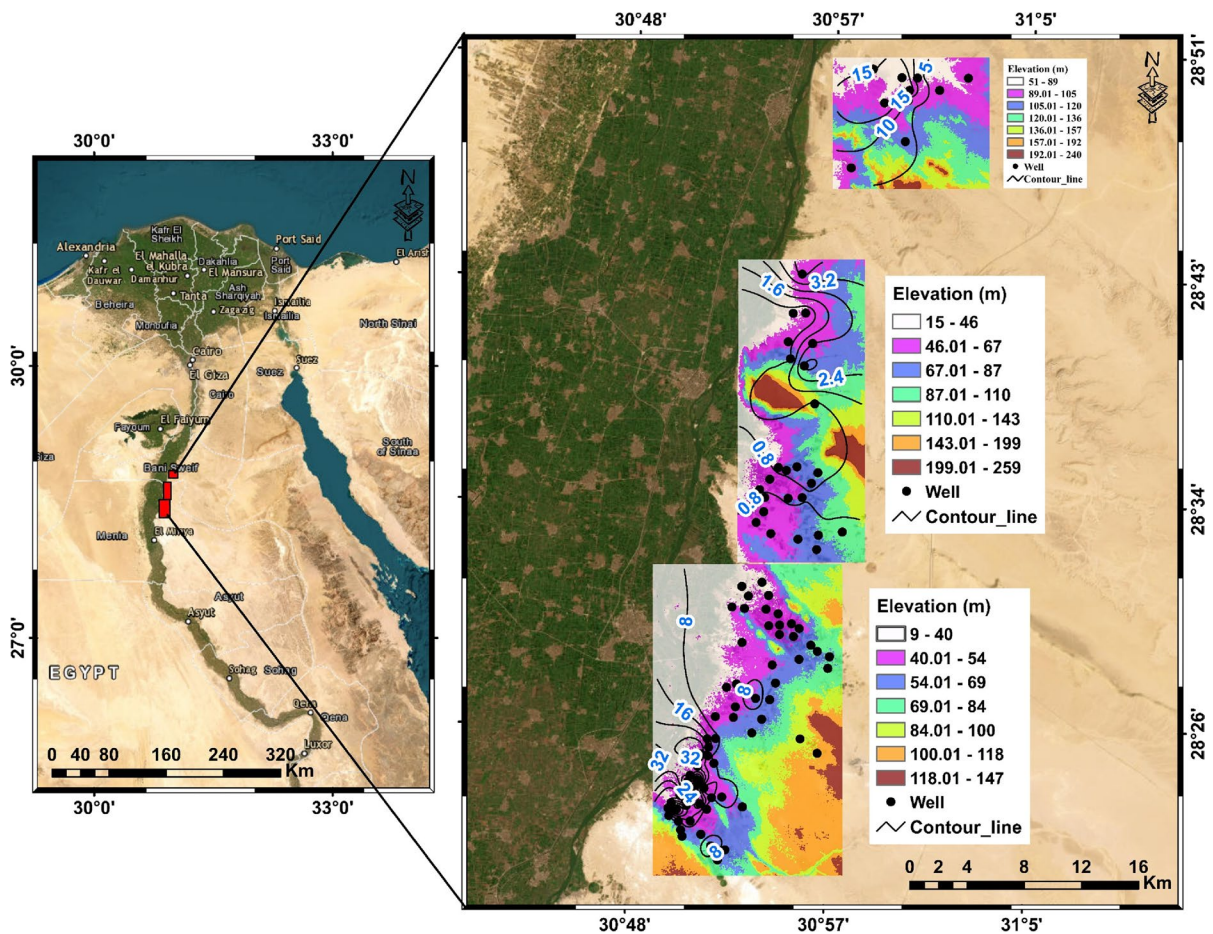


Fig. 1 Location map of the study area and water points plotted on SRTM DEM

an area of 289 km². The second zone (188 km²) is characterized by numerous low hills in its center and its elevation ranges from 15 to 259 m (asl). The third zone (100 km²) has an elevation ranged from 51 to 240 m (asl) (Fig. 1).

The climate of Egypt is characterized with hot/dry summer and mildly-wet/cold winter with average values of about 14°C and 30°C during winter and summer months, respectively (Elshaeb et al., 2014). These temperatures in the inland desert areas, however, fluctuate considerably, particularly during summer, from 7°C during night up to 43°C during day (Elshaeb et al., 2014). As the study area is located in arid zone and prevailing of dry wind, high evaporation rates are recorded, and they range from 4.8 mm/day in winters to 12.4 mm/day in summers (Harmsen, 2016; Khalil et al., 2021). Egypt receives extremely limited rainfall and the average precipitation rate

fluctuates from few millimeters in desert areas up to 260mm year⁻¹ in Sinai Peninsula (El Alfy & Merkel, 2006; Mahmoud, 2014). The annual precipitation rate of the studied area, however, ranges from 3 to >50 mm year⁻¹ (Egyptian Metrological Authority 1996). However, flash floods are the foremost natural risk since several moderate flash floods were recorded in the studied area during the last 50 years, especially in years of 1969, 1980, 1984, 1985, 1994 and 2020 (Abdel Moneim 2005; El-Saadawy et al., 2020).

2.2 Geology and Hydrogeology

The study area is characterized by a succession of Tertiary to Quaternary sedimentary rocks (Fig. 2). The middle Eocene Samalut Formation exposed in the southern part of the study area with thickness of 58m, it overlays the Minia Formation and

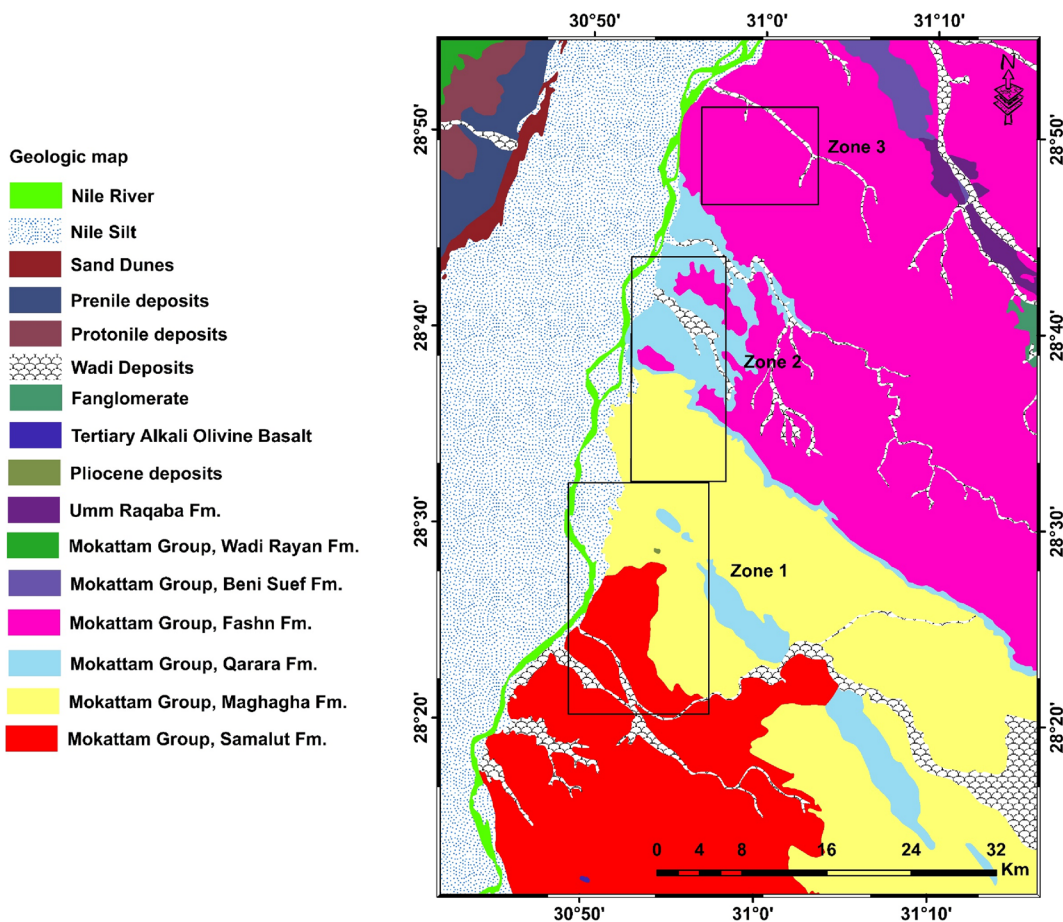


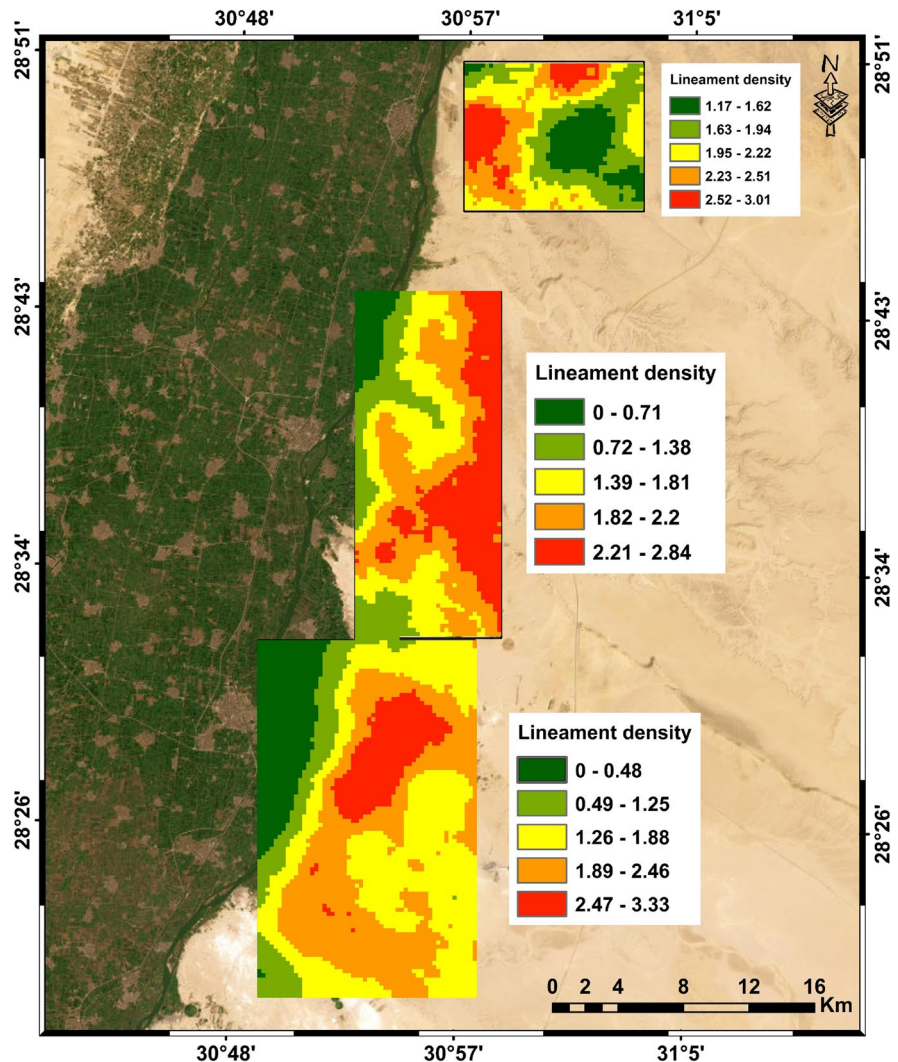
Fig. 2 Geologic map of the study area

undelaying Maghagha Formation. Its lower unit has thin-bedded, grayish white, soft-burrowed nummulitic limestone with calcareous shale at the base. Whereas, the upper unit involves pinkish white and massive to faintly graded bedding nummulitic limestone (Bishay, 1961; Said, 1960). The chalk-marl complex of middle Eocene Maghagha Formation conformably overlies the Samalut Formation and underlies the Qarara Formation with a succession of 100 to 160m thick east of Beni-Mazar and Maghagha cities (Bishay, 1966).

The limestone of middle Eocene Qarara Formation is unconformably underlain by the Middle Eocene Maghagha Formation. The lower part is composed of variably colored mudstone with

gypsum veinlets and siltstone lenses, while the upper part is a yellowish sandy, fossiliferous limestone and marl intercalations ((Bishay, 1966; Said, 1960). The middle Eocene Fashn Formation unconformably overlies the Qarara Formation. The lower part is bedded chalky limestone with chert nodules and bands that are overlain by shale with gypsum veinlets, while the upper part formed of yellowish white limestone intercalated with marl (Bishay, 1966). The Quaternary alluvium deposits are related to Wadi courses. These deposits consist of gravel, sand and silt; however, the Nile silt and clay are deposited in Nile Valley in the western part of the study area. The Fractured limestone Eocene aquifer is tested in the study area since it is influenced by a

Fig. 3 Map of the water Level for the study area

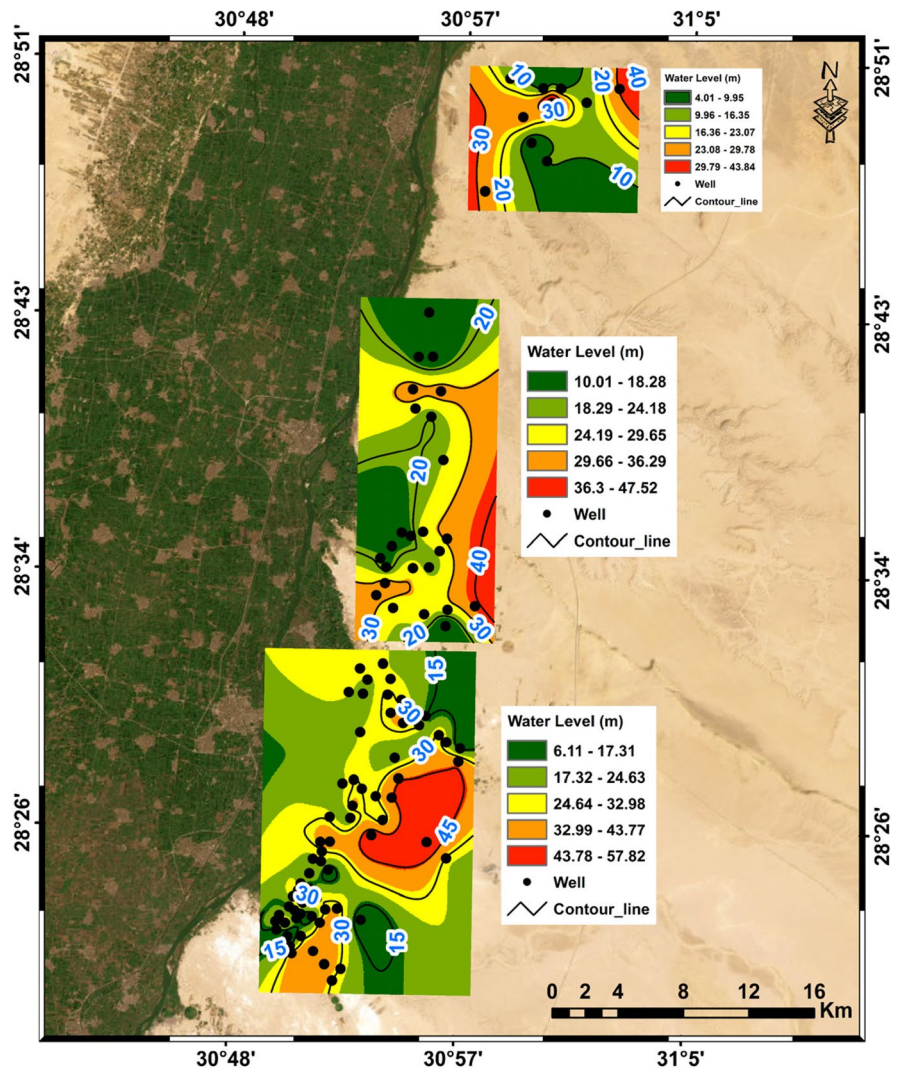


network of faults and might play an important role in groundwater recharge (Said, 1981). It is characterized by unconfined to semi-confined conditions, which overlain by permeable alluvium sediments. This aquifer has alternative layers of shale, marl, chert bands and nodules; therefore, it represents low hydraulic potential with effective porosity of 13% (Habibah et al., 2022; Tawab, 1994). The Eocene aquifer is recharged by infiltration of water during intense rainfall occasional flash flood events (Sultan et al., 2000) (Fig. 3). In addition, seepage from River Nile and irrigation/drainage canals can recharge this aquifer (Habibah et al. 2022) (Fig. 4).

2.3 Water Sampling and Analysis

Groundwater (104 samples) was collected in July 2022 (Fig. 1) with the finest spatial distribution using the techniques outlined by APHA 1995 and USGS 2007. Physicochemical characteristics of groundwater samples including temperature, dissolved oxygen (O₂), redox potential (Eh), hydrogen ion concentration (pH), total dissolved solid (TDS) and electrical conductivity (EC) were measured directly in the field using HQ40d Portable Multi-Parameters Meter. This was calibrated for each specific measurement using the proper

Fig. 4 Total Dissolved solids (TDS) in the sampled groundwater, expressed in (mg/L)



standard solution. Other chemical analyses of water samples were carried out at the Central Laboratories of National Water Research Center (NERC). Major cations calcium (Ca^{2+}), magnesium (Mg^{2+}), sodium (Na^+) and potassium (K^+) and anions chloride (Cl^-) and sulfate (SO_4^{2-}) were determined using ion chromatography method; however, bicarbonate (HCO_3^-) and fluoride (F^-) were measured by acid–base titration and ion selective electrode, respectively (Fig. 5). Trace elements concentration aluminum (Al^{3+}), barium (Ba^{2+}) chromium (Cr^{6+}), copper (Cu^+), iron (Fe^{2+}), manganese (Mn^{2+}), strontium (Sr^{2+}) and zinc (Zn^{2+}) were determined using ICP-MS (Inductively Coupled Plasma-Mass Spectrometer).

2.4 Hydrochemical Classification

To identify the key factors that impact hydrochemistry, it is crucial to identify the principal ions in groundwater (El Alfy et al., 2019; Karroum et al., 2017; Musaed et al., 2020; Narany et al., 2018). Gibbs (1970) put forth the idea of using TDS versus $\text{Cl}^-/(\text{Cl}^- + \text{HCO}_3^-)$ for anions and TDS versus $\text{Na}^+ / (\text{Na}^+ + \text{Ca}^{2+})$ for cations as a mean of illustrating the natural processes that govern groundwater chemistry. Other hydrochemical processes that could regulate groundwater quality including evaporation, precipitation, rock weathering, and rainfall recharge were also recorded (Honarbakhsh et al., 2019; Loni et al., 2015) (Fig. 6). A Piper diagram can be used

Fig. 5 Concentration levels of nitrates in the sampled groundwater in (mg/L)

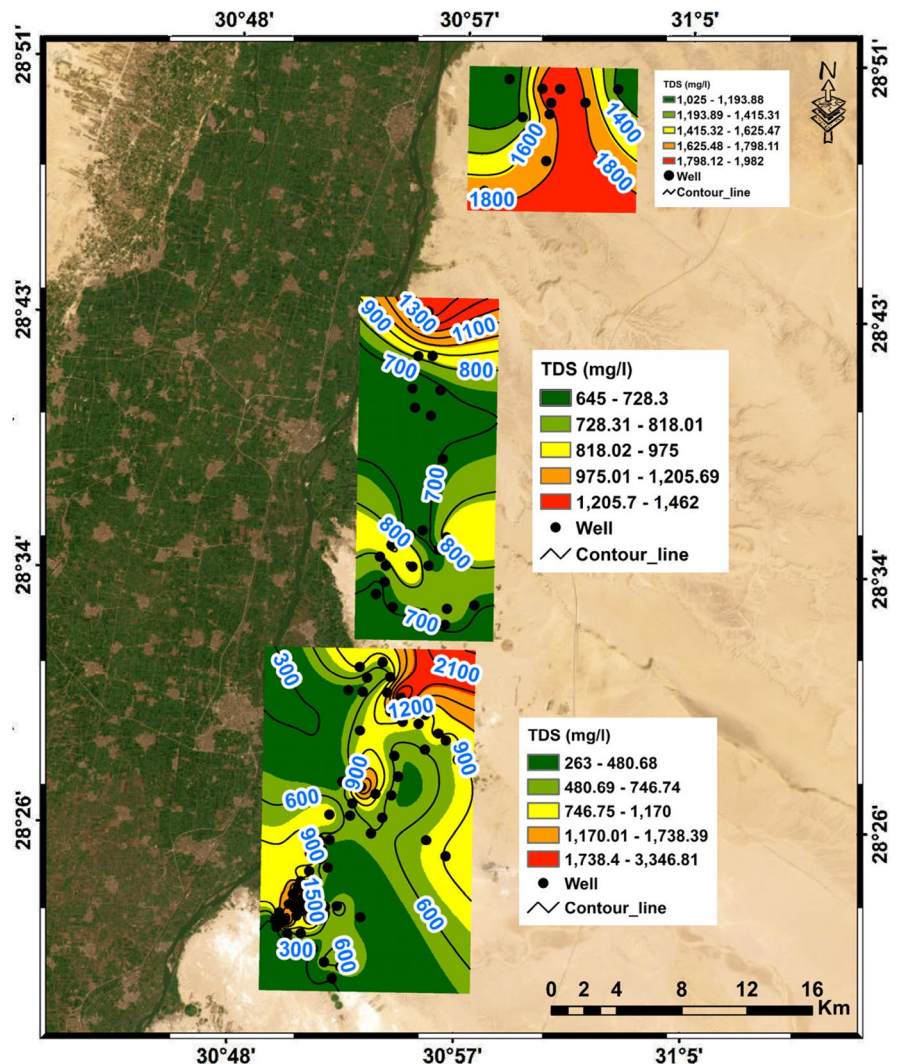
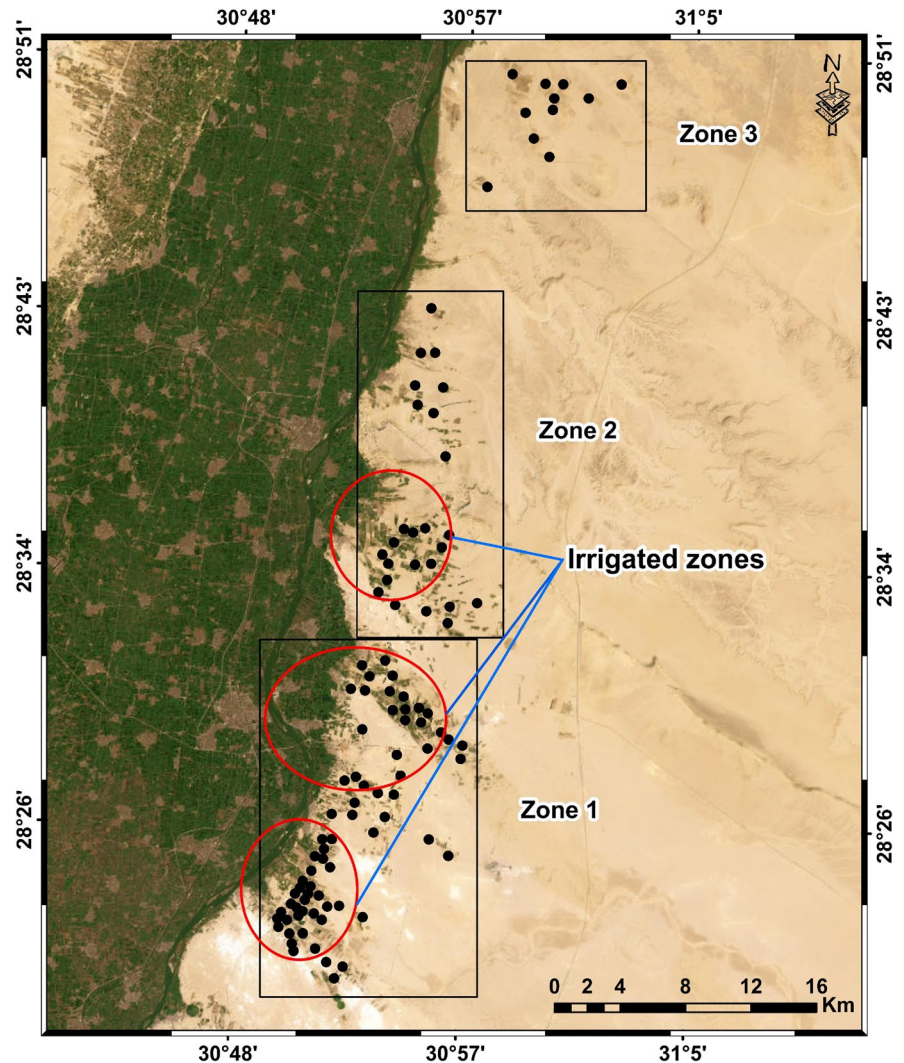


Fig. 6 Piper diagram for three locations a, b and c

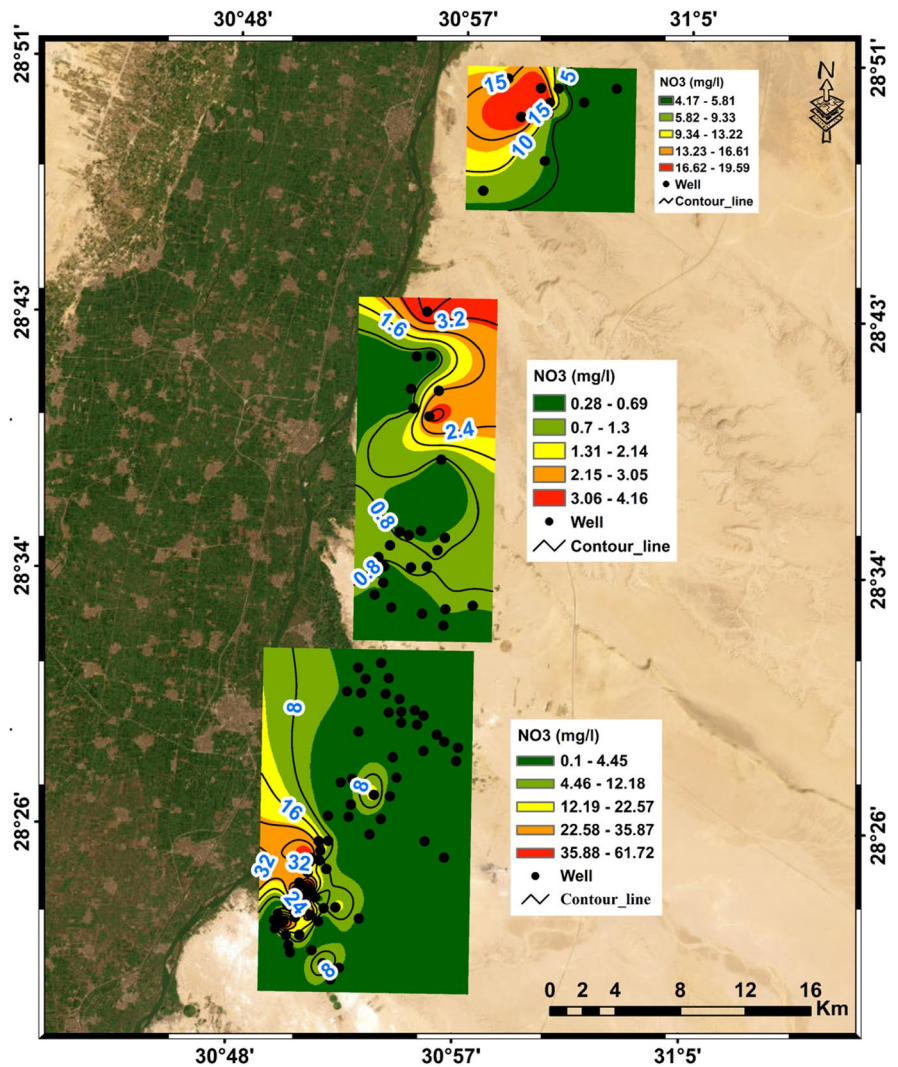


as helpful technique to illustrate the hydrochemical data to categorize various types of groundwater and understand the potential sources of the dissolved constituent salts in groundwater (Domenico & Schwartz, 1997; El Alfy & Merkel, 2006; Freeze & Cherry, 1979; Sargazi et al., 2021) (Fig. 7). Besides, Durov diagram was utilized to provide a comprehensive explanation of the hydrochemical processes that impact groundwater and identifying original genesis of groundwater resources (Al-Bassam & Khalil, 2012). Durov diagram can also investigate various water types in water mixtures as well as ion and reverse ion exchange processes (Lloyd & Heathcote, 1985).

2.5 Multivariate and Geostatistical Analyses

The use of multivariate statistical approaches in SPSS_{v25} is critical in detecting natural processes that impact groundwater and addressing hydrochemistry difficulties (Gulgundi & Shetty, 2018) (Fig. 8). The original data set was normalized prior to statistical analysis using the standards specified by (Davis, 2002). The geographical distributions of groundwater variables were modelled in a GIS system, while universal kriging was employed to assess parameter values in unmeasured sites. Pearson correlation coefficient was utilized to evaluate the degree of similarity between two parameters in order to examine the

Fig. 7 Drouve diagram for three locations a, b and c



hydrochemical evolution of groundwater (Nair et al., 2005; Unnisa & Zainab Bi, 2017; El Alfy et al., 2019).

2.5.1 Factor Analysis

Factor analysis was conducted to identify the significant factors contributing to groundwater hydrochemical processes and classify the various groundwater areas (Davis, 2002; Nan et al., 2016; El Alfy et al., 2017). A total of twenty-three hydrochemical variables were utilized to establish associations between the physicochemical characteristics of the water and identify correlations (Fig. 9). The amount

of variance explained by each variable was calculated by squaring the corresponding factor loading for each factor. The residual variance for each variable was computed by subtracting the sum of the variances explained by each factor from 100%. The maximized variance associated with factors was assessed using their eigenvalues, which serve as indicators of the significance of the factors. The factors with the highest eigenvalues are deemed the most significant, and any eigenvalues equal to or greater than 1.0 are considered being significant (Davis, 2002; Kim & Mueller, 1978). The extraction of the primary factors was accomplished using the varimax criterion (Kaiser, 1958), which enhanced

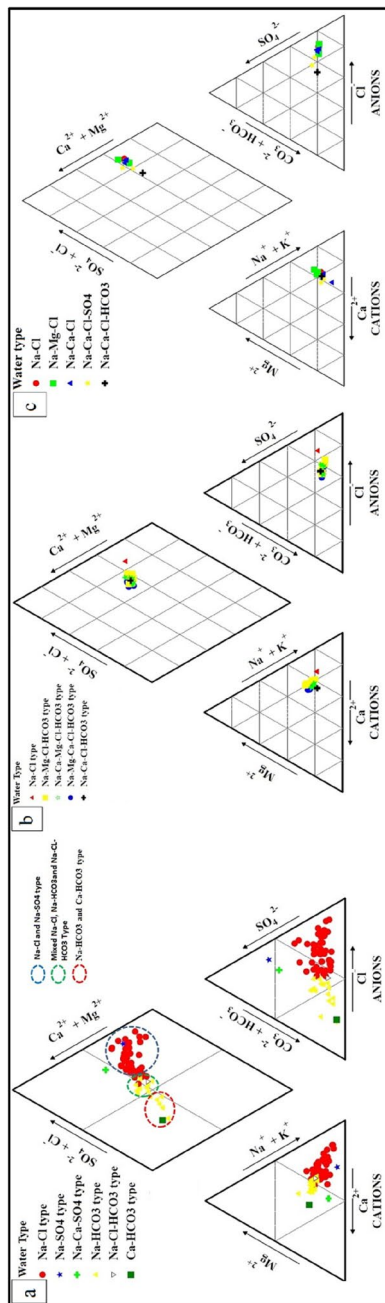


Fig. 8 Gibbs diagram for three locations a, b and c

the loadings of closely related variables within each factor. This approach facilitated the identification of easily interpretable components (Furi et al., 2012).

2.5.2 Claustal Analysis

Cluster analysis is performed to categorize the hydrochemical system into multiple minor hydrochemical regimes (Suk & Lee, 1999). Cluster analysis is an effective tool that can be utilized to examine and comprehend the groundwater hydrochemical system by discretizing different groundwater zones that hold geological significance (Fig. 10). Cluster analysis is employed to classify water chemistry data in distinct areas and geologic aquifers (Alther, 1979; El Alfy et al., 2018). The hydrochemical data were standardized using z-standardization to ensure equal weighting, and then the samples were grouped based on their similarity to one another. The data were normalized using the following equation to ensure that all variables have the same mean and standard deviation values (Davis, 2002).

$$Z_{ij} = (X_i - \mu_i) / \sigma_i \tag{1}$$

where X_i represents the data for the parameters i , μ_i and σ_i are the mean and the standard. Cluster analysis was conducted using 23 variables. The results provided logical values for data interpretations and hydrochemical patterns that accurately represent field conditions (Fig. 11).

2.6 Saturation Index

The saturation indices were utilized to estimate the reactivity of minerals in the groundwater. It is possible to predict the presence of reactive minerals in aquifer media by analyzing groundwater without the necessity of collecting solid phase samples for direct mineralogical analysis (Deutsch, 2020) (Table 1). The saturation index (SI) is a measurement of the interaction between groundwater and rock. The PHREEQC software was employed to calculate the SI values. The saturation index (SI) for a specific mineral can be defined as follows:

$$SI = \log \frac{KIAP}{K_{sp}} \tag{2}$$

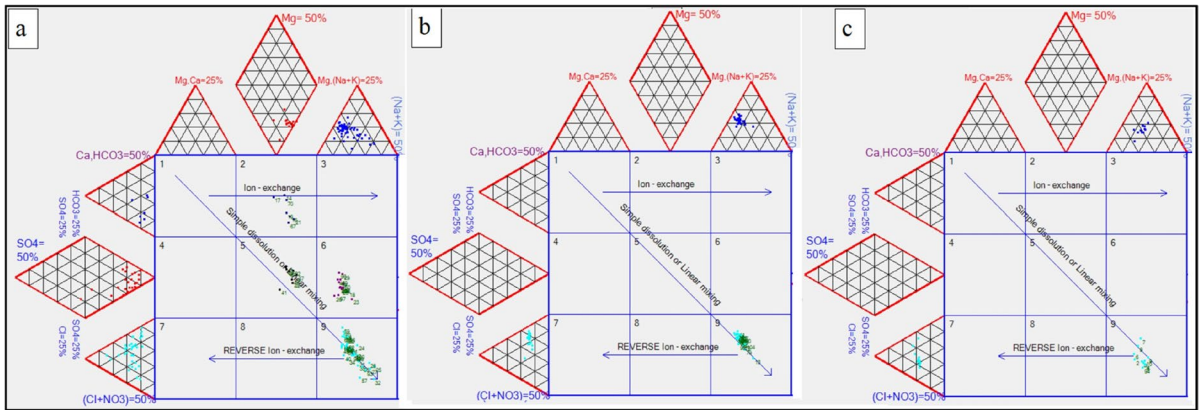


Fig. 9 a: 3D representation of loadings of Factor 1, factor 2 and factor 3 after varimax rotation. B: 3D representation of loadings of Factor 4, factor 5 and factor 6 after varimax rotation. (zone 1)

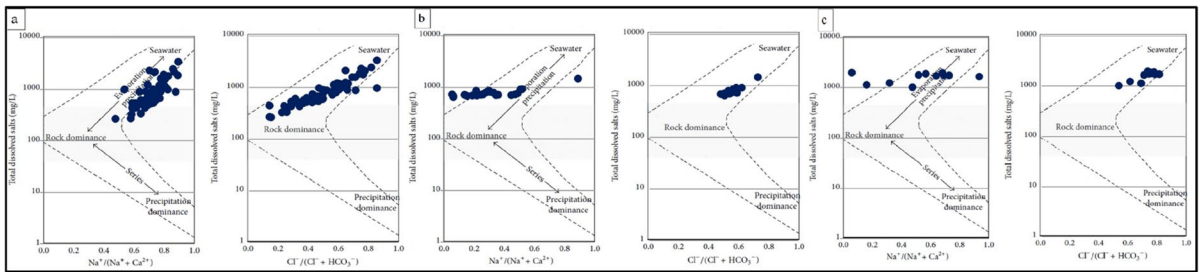


Fig. 10 a: 3D representation of loadings of Factor 1, factor 2 and factor 3 after varimax rotation. B: 3D representation of loadings of Factor 4, factor 5 and factor 6 after varimax rotation. (zone 2)

where K_{IAP} is the ion activity product, and K_{sp} is the solubility product with respect to the temperature of the water sample (Table 2). When the saturation index (SI) is positive, it indicates that there is supersaturation or the possibility of precipitation of secondary minerals. A negative saturation index (SI) indicates undersaturation, meaning that the dissolution of minerals is necessary to attain equilibrium. A saturation index of 0.5 signifies equilibrium conditions (Parkhurst & Appelo, 1999).

3 Results and Discussion

3.1 Spatial Data Distribution

One hundred and four samples were collected from the study area (Table 3). Based on the lineament

map, cluster analysis, water types, and geologic map, the study area was divided into three zones. The first zone has a high lineament density in its central part, the second zone exhibits a similar high density in its eastern part, while the third zone has high lineament density in the western and northern parts (Appendix Fig. 13). The first zone is situated in the southern part of the study area and comprises sixty-eight groundwater samples (Fig. 3). The depth to water in this zone ranges from 4 to 75m, while the total depth of the wells ranges from 20 to 227m. Additionally, the water level in wells varies from 6 to 58m (Fig. 3). The second zone is located between the two other zones and consists of twenty-five groundwater samples (Fig. 3). The depth to water in this zone varies from 22 to 90m, and the total well depth ranges from 120 to 370m. Additionally, the water level in wells ranges from 10 to 56 m (Fig. 3). The third zone is positioned

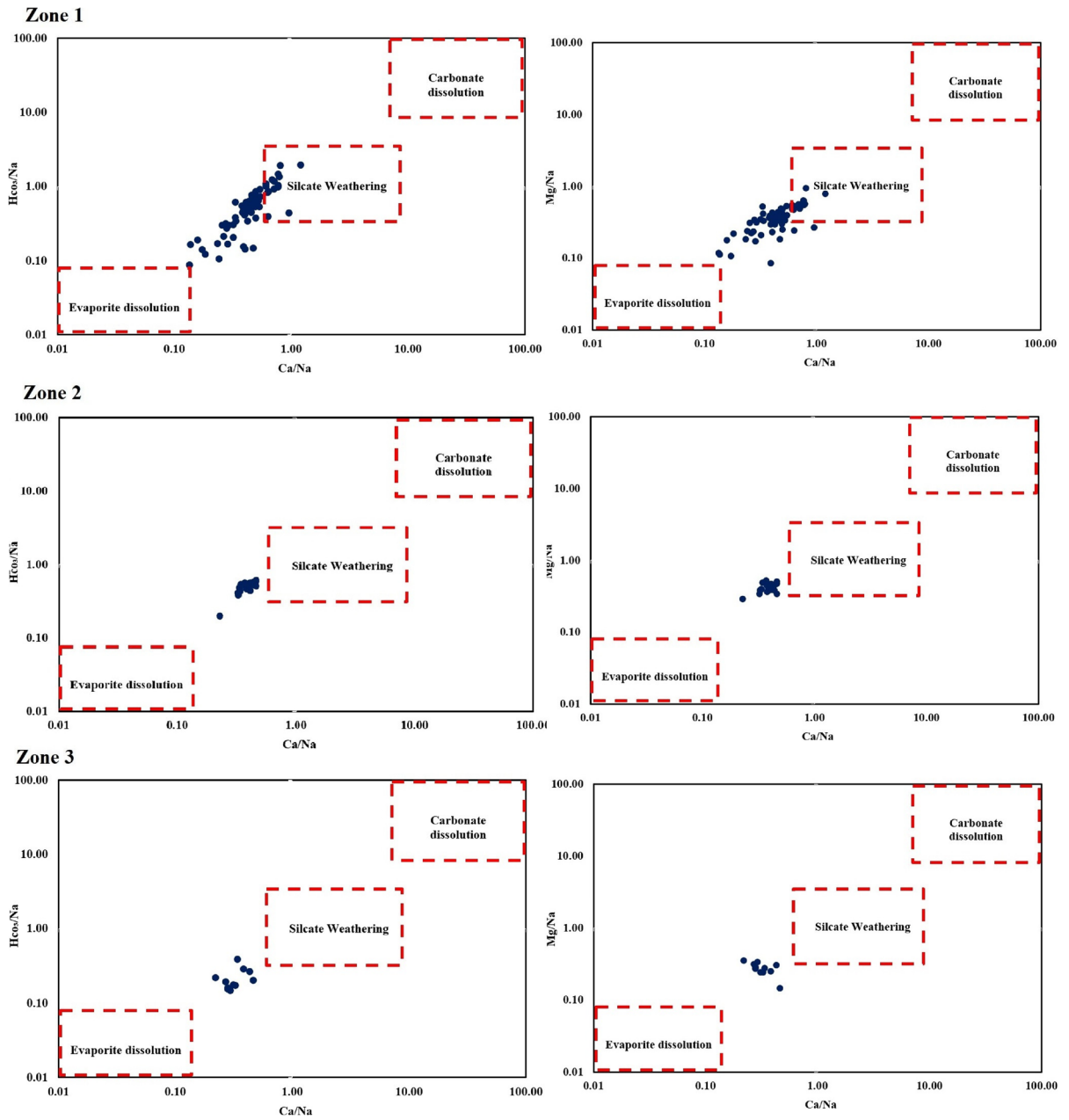


Fig. 11 a: 3D representation of loadings of Factor 1, factor 2 and factor 3 after varimax rotation. b: 3D representation of loadings of Factor 4, factor 5 and factor 6 after varimax rotation. (zone 3)

Table 1 Salinity value of the different clusters (Zone 1)

Clustal NO	Parameters	Minimum	Maximum	Mean	Std. Deviation
Clustal I	TDS	980	3370	2019	579
Clustal II	TDS	786	1260	987	190
Clustal III	TDS	431	1,210	742	247
Clustal IV	TDS	263	679	475	128
Clustal V	TDS	270	1166	701	206

in the northern part of the study area and comprises eleven groundwater samples (Fig. 3). The depth to water in this zone ranges from 50 to 100m, while the total well depth varies from 96 to 400m. Additionally, the water level in the wells ranges from 4 to 44 m (Fig. 3). It is important to note that the depth to the water table increases from the southern to the northern part of the large study area. It is noticed that groundwater salinity increases northeastward, where the groundwater becomes deeper. Meanwhile, shallow groundwater with low salinity is recorded in the south and west areas, where the aquifer is recharged with fresh Nile water.

3.2 Salinity Distribution

Groundwater quality was characterized by low to moderate salinity levels with TDS values ranging from 263 to 3370 mg L⁻¹ and average of 924 ± 603.39 mg L⁻¹. Forty-five samples (66%) were above the

desirable limit of WHO 2017(600 mg L⁻¹). Those areas with high TDS values were primarily observed in the north-east, south-west, and central parts of the study area (Fig. 4 and Fig. 12). The second zone is characterized by moderate to high salinity, with TDS concentrations ranging from 645 to 1462 mg L⁻¹ and averaged as 773 ± 160.92 mg L⁻¹. All the sample values (100%) exceeded the permissible limit prescribed by WHO 2017 (600 mg L⁻¹), indicating that the water in this zone is unsuitable for drinking. The highest values of TDS were observed in the northern part, with smaller concentrations also present in the western and eastern regions of the study area (Fig. 4). The third zone exhibited the highest salinity levels. The TDS values in this zone ranged from 1025 to 1982 mg L⁻¹, with a mean of 1629 mg L⁻¹. Values of all sample exceeded the desirable limit set by WHO 2017 (600 mg L⁻¹), indicating that the water in this zone is unsuitable for drinking. The high concentrations of TDS extended from the northern to southern parts, indicating a discharge area, while the low values were observed in the western and eastern parts of the study area, suggesting recharge sources from the Nile River and rainfall (Fig. 4). Based on the salinity results, it was observed that the salinity increased towards the north with increasing groundwater depth. The elevated TDS values were associated with geogenic processes, specifically water–rock interactions, where groundwater deeply percolated and dissolved aquifer minerals when it flows from the Red Sea hills to reach the Nile valley. This leads to higher ion concentrations in groundwater, such as the dissolution of evaporite

Table 2 Salinity value of the different clusters (Zone 2)

Clustal NO	Parameters	Minimum	Maximum	Mean	Std. Deviation
Clustal I	TDS	688	855	737	79.52
Clustal II	TDS	709	912	816	88.41
Clustal III	TDS	645	810	715	45.11

Table 3 Salinity value of the different clusters (Zone 3)

Clustal NO	Parameters	Minimum	Maximum	Mean	Std. Deviation
Clustal I	TDS	1025	1242	1136	108.64
Clustal II	TDS	1893	1982	1937	62.93
Clustal III	TDS	1663	1938	1780	100.32

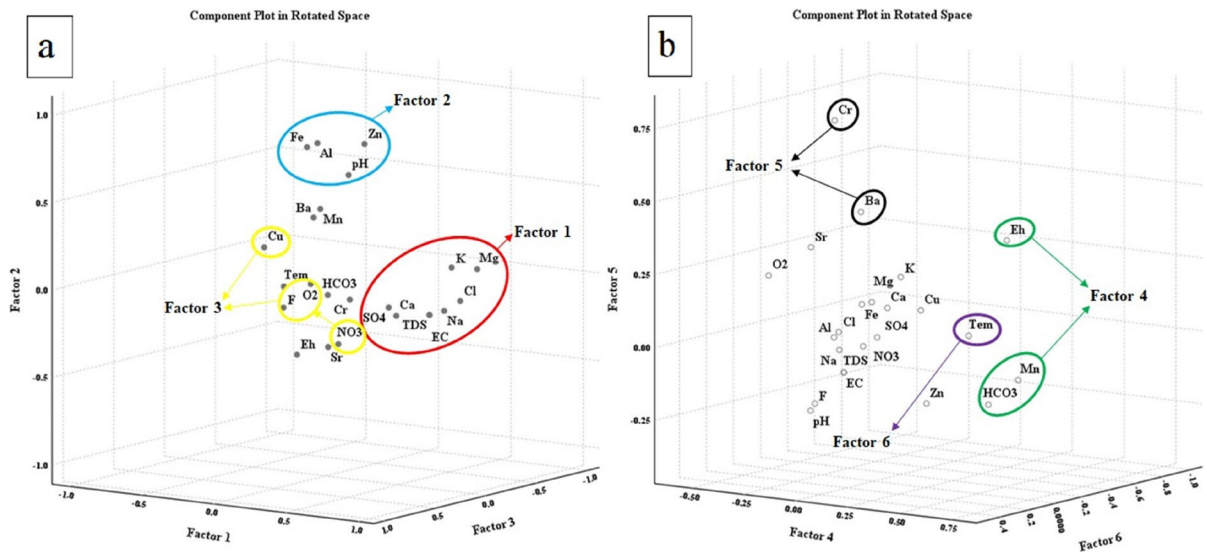


Fig. 12 Clustal analysis for three location a, b and c

and carbonate rocks, as well as ion exchange. Additionally, anthropogenic processes, such as irrigation return flow, contributed to the increased salinity levels in the groundwater, spatially in the irrigated area with groundwater (Appendix Fig. 14).

3.3 Groundwater Contamination with Nitrate

Values of NO_3^- in the first zone ranged from 0.10 to 61.8 mg L^{-1} with a mean of 10.01 mg/l (Fig. 13). Only two samples (3%) exceeded the permissible limit prescribed by WHO 2017 (50 mg/l). The eastern part of this zone exhibited the highest concentrations of NO_3^- (Fig. 5). Meanwhile, all samples of NO_3^- in the second zone were within the desirable limit of WHO and their values ranged from 0.28 to 4.16 NO_3^- , with an average of 0.99 mg L^{-1} . The highest concentrations of NO_3^- were observed in the north and north-east parts of this zone (Fig. 5). Values of NO_3^- in the third zone were further within the permissible limit prescribed by WHO with a range of 4.17–19.65 mg L^{-1} and average value of 10.54 mg L^{-1} . The highest NO_3^- concentrations, however, were observed in the north-western part of this zone (Fig. 5). It could be observed that agricultural activities are the most important source influencing groundwater quality in the first zone since it is close to the Nile River and characterized by shallow depth and flood irrigation. The higher concentration of nitrate is recorded in the

south with shallow low TDS groundwater (Fig. 4 and Fig. 5). However, NO_3^- concentrations decreased towards the north, where the groundwater depth increased and the nitrate is oxidized during its flow through the vadose zone (excess of oxygen).

3.4 Groundwater Origin and Hydrochemical Facies

3.4.1 Piper Diagram

Piper diagram was used in order to determine the main hydrochemical facies. In the first zone, three distinct hydrochemical facies, comprising six diverse groundwater types, were identified (Fig. 6a and Fig. 14). The majority of groundwater samples (72%) belonged to the $\text{Na}^+\text{-Cl}^-$ type (facies); however, only one sample (1.4%) was related to the $\text{Na}^+\text{-SO}_4^{2-}$ type, and another sample (1.4%) was related to the $\text{Na}^+\text{-Ca}^{2+}\text{-SO}_4^{2-}$ type. Fifteen groundwater samples (22%) were categorized as $\text{Na}^+\text{-HCO}_3^-$ type. However, only one sample (1.4%) was related to the $\text{Na}^+\text{-Cl}^-\text{-HCO}_3^-$ type and another one (1.4%) was classified as $\text{Ca}^{2+}\text{-HCO}_3^-$ type. Meanwhile, five different groundwater types were identified in the second zone (Fig. 6b). Only one groundwater sample (4%) belonged to the $\text{Na}^+\text{-Cl}^-$ type. Water types are categorized as transitional or mixed types, starting from $\text{Na}^+\text{-Mg}^{2+}\text{-Cl}^-\text{-HCO}_3^-$ types (seven samples, 28%), followed by $\text{Na}^+\text{-Ca}^{2+}\text{-Mg}^{2+}\text{-Cl}^-\text{-HCO}_3^-$ types (five

samples, 20%), $\text{Na}^+\text{-Mg}^{2+}\text{-Ca}^{2+}\text{-Cl}^-\text{-HCO}_3^-$ (eleven samples, 44%), and $\text{Na}^+\text{-Ca}^{2+}\text{-Cl}^-\text{-HCO}_3^-$ (one sample, 4%). Five water types were identified in the third zone, in which two samples (18%) were related to $\text{Na}^+\text{-Cl}^-$ type and the other three samples (27%) belonged to the $\text{Na}^+\text{-Mg}^{2+}\text{-Cl}^-$ type (Fig. 6c). Additionally, the $\text{Na}^+\text{-Ca}^{2+}\text{-Cl}^-$ type was represented by three samples (27%), with Ca^{2+} being present but Mg^{2+} absent. Furthermore, there were two samples (18%) of the $\text{Na}^+\text{-Ca}^{2+}\text{-Cl}^-\text{-SO}_4^{2-}$ type, or mixed types, in which SO_4^{2-} was present. Finally, one groundwater sample belonged to the $\text{Na}^+\text{-Ca}^{2+}\text{-Cl}^-\text{-HCO}_3^-$ type. These types indicate certain hydrochemical processes, such as the dissolution of evaporate and carbonate rocks (including anhydrite, gypsum, halite, calcite, and dolomite) and ion exchange.

3.4.2 Drouve Diagram

The groundwater samples of the first zone were categorized into four fields (NO. 2, 5, 6, and 9) (Fig. 7a). Seven samples (10%) fell into the $\text{Mg}^{2+}\text{-HCO}_3^-$ facies, indicating influence from meteoric groundwater recharge. Eight samples (12%) were plotted along the dissolution or mixing line, suggesting the mixing of groundwater from two or more different facies. This observation suggested the presence of two different sources of groundwater, possibly from the Nile River and rainfall precipitation. Seventeen samples (25%) were classified as $\text{Na}^+\text{-SO}_4^{2-}$ facies, indicating gypsum and halite dissolution. These facies may form when the excess Na^+ , after its connection with Cl^- , pairs with the excess SO_4^{2-} , left after its connection with Ca^{2+} and Mg^{2+} . Thirty-six samples (52%) fell into the $\text{Na}^+\text{-Cl}^-$ facies, which points to ion exchange and high halite dissolution, a conclusion supported by the saturation index. In the second and third zones, all groundwater samples fell into field NO. 9 and were plotted along the dissolution or mixing line, indicating the mixing of groundwater from two or more different facies (Fig. 7b, c). This suggests the presence of two distinct

sources of groundwater or mixed water, likely originating from the Nile River and rainfall. Furthermore, the dissolution of evaporate and carbonate rocks, as well as ion exchange, played a significant role in shaping the chemical composition of the groundwater samples.

3.4.3 Saturation Indices and Geochemical Processes

The average saturation index values of the existing minerals, such as anhydrite, halite, and gypsum mineral phases, were negative. This finding pointed to the dominance of under-saturation conditions for these minerals (Table 4). These minerals tend to be in the dissolved phases, leading to the expansion of open spaces and fractures in the aquifer. As a result, the porosity and permeability of the aquifer increase, facilitating better groundwater flow and storage. While the Saturation Index (SI) of dolomite and calcite was above saturation conditions, indicating the precipitation of secondary minerals. This observation provides valuable information about the flow of water, which was from the south to the north.

Data presented on the Gibbs diagram (Fig. 8a, b, and c) demonstrate the relationship between $(\text{Na}^+ + \text{K}^+)/(\text{Na}^+ + \text{K}^+ + \text{Ca}^{2+})$ versus TDS and $(\text{Cl}^-)/(\text{Cl}^- + \text{HCO}_3^-)$ versus TDS. This diagram reveals the mechanism governing groundwater chemistry. In the first zone, the groundwater samples fall along a transition zone between rock dominance and evaporation dominance (Fig. 8a). This indicates that both of these processes play an important role in governing the groundwater chemistry. However, since the depth of groundwater in this zone is above 20m, the influence of evaporation on groundwater chemistry must be minimal. Therefore, rock-water interaction is the main dominating factor influencing groundwater chemistry in this area. In the second zone, the majority of samples (96%) fall within the region dominated by rock-water interaction (Fig. 8b). Only one sample was in the region of evaporation precipitation. This indicates that the chemical compositions of groundwater in this zone

Table 4 Average cluster saturation indices (SI) of the different mineral phases

parameters	Anhydrite	Halite	Gypsum	Dolomite	Calcite
Mean (zone 1)	-1.93	-5.86	-1.65	2.29	1.13
Mean (zone 2)	-2.03	-5.82	-1.77	2.47	1.15
Mean (zone3)	-1.50	-5.16	-1.24	1.50	0.73

are primarily influenced by rock-water interaction. In the third zone, the majority of samples fall within the region of evaporation precipitation (Fig. 8c). However, since the depth to groundwater in this zone is above 90m, the influence of evaporation on groundwater chemistry must be minimal. Consequently, rock-water interaction remains the main dominating factor influencing groundwater chemistry in this area.

The relations between $\text{Ca}^{2+}/\text{Na}^+$ vs $\text{HCO}_3^-/\text{Na}^+$ and $\text{Ca}^{2+}/\text{Na}^+$ vs $\text{Mg}^{2+}/\text{Na}^+$ were established. It was found that in all three zones, groundwater chemistry is primarily influenced by silicate weathering and evaporation dissolution. (Appendix Fig. 15).

3.4.4 Multivariate Statistics

Pearson Correlation coefficient matrix was computed for the hydrochemical parameters. In the first zone, the hydrochemical parameters O_2 , Eh, temperature and pH exhibited negative and poor correlation with all other parameters (Appendix Table 5). However, strong correlations were observed between TDS and EC with Ca^{2+} , Na^+ , Cl^- , and SO_4^{2-} , as well as moderate correlations with K^+ , Mg^{2+} , and NO_3^- . Moreover, there was a strong correlation between Ca^{2+} and Na^+ , NO_3^- , and SO_4^{2-} , and a moderate correlation with K^+ , Mg^{2+} , and Cl^- . Additionally, K^+ displayed a strong correlation with Mg^{2+} and Cl^- , and a moderate correlation with Na^+ and SO_4^{2-} . Likewise, Mg^{2+} showed a strong correlation with Na^+ and Cl^- , while Na^+ exhibited strong and moderate correlations with Cl^- and SO_4^{2-} , respectively. Furthermore, Cl^- demonstrated a moderate correlation with SO_4^{2-} and NO_3^- displayed a strong correlation with SO_4^{2-} . On the other hand, pH showed negative correlations with all other parameters.

In the second zone, the hydrochemical parameters (O_2 , Eh, and pH) exhibited negative and poor correlation with all other parameters (Appendix Table 6). However, temperature showed a strong correlation with F^- and NO_3^- , and a moderate correlation with TDS and EC. Furthermore, TDS and EC demonstrated strong correlations with Ca^{2+} , Mg^{2+} , Na^+ , F^- , Cl^- , and SO_4^{2-} , as well as moderate correlations with NO_3^- . Additionally, a strong correlation was observed between Ca^{2+} and Na^+ , and Ca^{2+} with Cl^- , while a moderate correlation existed between Ca^{2+} and K^+ and F^- . Fluoride F^- showed strong correlations with Cl^- , NO_3^- , and SO_4^{2-} , and a moderate correlation with Ca^{2+} and Cl^- . Moreover, Mg^{2+}

displayed strong correlations with Na^+ , F^- , Cl^- , and SO_4^{2-} , and a moderate correlation with NO_3^- . Similarly, Na^+ had a strong correlation with F^- , Cl^- , and SO_4^{2-} . Additionally, Cl^- exhibited a strong correlation with SO_4^{2-} . Furthermore, a strong correlation was observed between Cr^{6+} and Si^{2+} , and a moderate correlation with Fe^{2+} .

In the third zone, O_2 displays a moderate correlation with TDS, Mg^{2+} , Na^+ , and Cl^- (Appendix Table 7). However, Eh shows poor correlation with all other parameters. The temperature exhibits a moderate correlation with Ca^{2+} and Al^{3+} , while the pH shows a strong correlation with K^+ , Fe^- , and Zn^{2+} , and a moderate correlation with Mg^{2+} , Cl^- , and Al^{3+} . Additionally, EC and TDS demonstrate strong correlations with Na^+ , Cl^- , and SO_4^{2-} , and a moderate correlation with Ca^{2+} , K^+ , Mg^{2+} , Cr^{6+} , and Cu^+ . Ca^{2+} shows strong correlations with SO_4^{2-} and Al^{3+} , and a moderate correlation with Na^+ , Cl^- , Cr^{6+} , Cu^+ , and Mn^{2+} . K^+ exhibits strong correlations with Cl^- , Fe^- , and Zn^{2+} , and a moderate correlation with Mg^{2+} , Na^+ , SO_4^{2-} , and Al^{3+} . Moreover, Mg^{2+} also has a moderate correlation with Na^+ and Cl^- , while Na^+ shows a strong correlation with Cl^- and SO_4^{2-} . While F^- and NO_3^- display negative correlations with most of the parameters.

Based on the previous correlation analysis, it is evident that TDS, being the summation of all dissolved components in groundwater, shows a strong correlation with the majority of the major ions. Moreover, the increasing values of EC are associated with higher TDS values, indicating a very strong correlation between these two parameters. The strong correlation of Ca^{2+} with Na^+ , Cl^- , and SO_4^{2-} , and the moderate correlation with Mg^{2+} , highlights the significant contribution of gypsum, halite, and dolomite dissolution in the chemical composition of groundwater. Additionally, the positive correlations between K^+ with Mg^{2+} , Na^+ , Cl^- , and SO_4^{2+} in the first and third zones indicate that these minerals are popular sources contributing to the groundwater composition. Notably, the major source of K^+ in groundwater primarily comes from surface discharges, which underscores the significant contribution of surface sources to the presence of this mineral in groundwater. Furthermore, the strong correlation between Mg^{2+} with Na^+ and Cl^- indicates ion exchange of minerals between rocks and water. Moreover, the strong correlation of Na^+ with Cl^- and SO_4^{2-} may be associated with a

long history of evaporation, suggesting the dissolution of gypsum and halite. Although the major ions also show relatively strong correlations with each other, it may not necessarily be related to the same geochemical processes. For instance, the increase in the concentration of SO_4^{2-} with Na^+ , Cl^- with F^- , and NO_3^- with SO_4^{2-} may not originate from the same sources. On the other hand, the trace elements displayed poor correlation with all other parameters, except for a moderate correlation between Fe^- and Al^{3+} . The main sources of these trace elements in the aquifer are likely attributed to the weathering of rocks bearing these minerals.

3.4.5 Factor Analysis

Twenty-three variables (O_2 , Eh, Tem, pH, EC, TDS, Ca^{2+} , K^+ , Mg^{2+} , Na^+ , F^- , Cl^- , NO_3^- , SO_4^{2-} , HCO_3^- , Al^{3+} , Ba^{2+} , Cr^{6+} , Cu^+ , Fe^{2+} , Mn^{2+} , Sr^{2+} , and Zn^{2+}) were analyzed, and the factors, eigenvalues, proportion of variance, and rotated factor loadings were explained.

In the first zone, the factor analysis shows six important factors with eigenvalues > 1 (Appendix Table 8). The factors represent a total variance of 73.50%, with the smallest eigenvalue being 1.045 (Appendix Table 8). Factor 1 accounted for about 28.57% of the total variance and had an eigenvalue of 7.48 (Appendix Table 8). It exhibited strong loadings with EC, TDS, Ca^{2+} , K^+ , Mg^{2+} , Na^+ , Cl^- , and SO_4^{2-} (Appendix Table 8 and Fig. 9a), ranging from 0.715 to 0.933. This factor indicates the influence of geogenic processes on the chemical composition of groundwater, such as the dissolution of gypsum, halite, dolomite, calcite, and ion exchange. Factor 2 accounted for 12.60% of the total variance and had an eigenvalue of 3.02 (Appendix Table 8). It displayed high to moderate loadings with pH, Al^{3+} , Fe^{2+} , and Zn^{2+} , with values of 0.579, 0.793, 0.809, and 0.760, respectively (Appendix Table 8 and Fig. 9a). This factor indicates an association with the alkaline nature and the processes of iron ion dissolution and precipitation. Factor 3 accounted for 11.97% of the total variance and had an eigenvalue of 2.09 (Appendix Table 8). It showed moderate loadings with O_2 , F^- , NO_3^- , and Cu^+ , with values of 0.508, 0.753, 0.641, and 0.616, respectively (Appendix Table 8 and Fig. 9a). This factor confirms that an oxygenated environment contributes to higher nitrate concentrations. The lithology of the study region alone does not fully

explain the raised concentration of fluoride. Instead, factors such as the leakage of fluoride-bearing minerals, concentrated irrigation practices, and the presence of clay minerals likely contributed to the high fluoride loadings. Similarly, the lithologic sources in the study area do not significantly contribute to the increased concentration of nitrate. Instead, the main source of nitrate was identified as the irrigation return flow. Factor 4 accounts for 8.67% of the total variance and has an eigenvalue of 1.91 (Appendix Table 8). It exhibits moderate loadings with Eh, HCO_3^- , and Mn^{2+} , having values of 0.574, 0.699, and 0.664, respectively (Appendix Table 8 and Fig. 9b). This factor is associated with the interaction of water and its surrounding environments, involving chemical and biological processes corresponding to the aquifer redox sequences. The moderate loading of HCO_3^- suggests meteoric groundwater recharge. The inverse relationship between Eh and pH reflects redox reactions, including nitrogen extractions, as higher pH values can promote these processes. This can be clearly observed from the high positive loading on Eh and the negative loading on pH. Factors 5 and 6 accounted for 6.26% and 5.43% of the total variance, with eigenvalues of 1.35 and 1.04, respectively (Appendix Table 8). Factor 5 exhibited moderate and high loadings with Ba^{2+} and Cr^{6+} , having values of 0.53 and 0.76, respectively (Appendix Table 8 and Fig. 9b). These significant loadings of Ba^{2+} and Cr^{6+} indicate weathering of mineral-bearing layers. On the other hand, Factor 6 showed only a negative loading with temperature, with a value of -0.839. This factor suggests that the temperature was less influenced by human activities and may be indicative of cool recharge water mixing with the aquifer water.

In the second zone, six factors were determined, all having eigenvalues > 1 (Appendix Table 9). These factors account for a total variance of 83.31%, with the smallest eigenvalue being 1.09 (Appendix Table 9). Factor 1 explains the largest portion of the variance, accounting for 32.33% of the total variance and an eigenvalue of 8.60 (Appendix Table 9). It exhibits strong loadings with EC, TDS, Mg^{2+} , Na^+ , F^- , Cl^- , and SO_4^{2-} , and moderate loadings with Ca^{2+} and NO_3^- (Appendix Table 9 and Fig. 10a). This factor suggests significant hydrochemical processes or geogenic influences, including ion exchange and the dissolution of gypsum, halite, anhydrite, calcite, and dolomite. The presence of nitrates in groundwater is mainly ascribed to agricultural fertilizer usage. The

moderate loading of NO_3^- indicates the impact of return irrigation flow. Moreover, this factor implies that human activities play a significant role in governing the chemical composition of groundwater in this zone. Factor 2 emphasizes the significant influence of Nile and rainfall water on groundwater recharge, as evidenced by its strong loading with pH and moderate loading with HCO_3^- , which typically occur under alkaline conditions (Appendix Table 9 and Fig. 10a). This factor explains 15.59% of the total variance and has an eigenvalue of 3.43 (Appendix Table 9). Furthermore, it indicates the dissolution of HCO_3^- in the aqueous phase and its subsequent precipitation as CO_3^{2-} in the solid phase. Factor 3 accounts for 12.92% of the total variance and has an eigenvalue of 2.82 (Appendix Table 9). It exhibits high loadings with Cr^{6+} , Fe^{2+} , and Sr^{2+} (Appendix Table 9 and Fig. 10a), indicating the weathering of layers containing these minerals. On the other hand, Factor 4 accounts for 8.87% of the total variance and has an eigenvalue of 1.77 (Appendix Table 9). It shows high loadings with Mn^{2+} and Zn^{2+} , along with a moderate loading with K^+ (Appendix Table 9 and Fig. 10b). This factor is associated with the weathering of clay minerals from surface recharge and the bearing layers of Mn^{2+} and Zn^{2+} . Additionally, it may also be influenced by agricultural activities involving the use of potassium and agricultural pollution. Factor 5 accounts for 6.96% of the total variance and has an eigenvalue of 1.46 (Appendix Table 9). It exhibits a strong loading with Eh and a moderate loading with Al^{3+} (Appendix Table 9 and Fig. 8b). On the other hand, Factor 6 explains 6.65% of the total variance and has an eigenvalue of 1.09 (Appendix Table 9). It shows high loading with Cu^+ and a moderate loading with Ba^{2+} (Appendix Table 9 and Fig. 10b). This factor suggests the weathering of layers containing these minerals, which could be attributed to geogenic and anthropogenic sources.

In the third zone, five factors were identified, all having eigenvalues > 1 (Appendix Table 10). These factors account for a total variance of 89.88%, with the smallest eigenvalue being 1.64 (Appendix Table 10). Factor 1 explains a significant portion of the variance, accounting for 29.14% of the total variance and having an eigenvalue of 8.69 (Appendix Table 10). It exhibits strong loadings with O_2 , EC, TDS, Na^+ , Cl^- , and SO_4^{2-} , and moderate loadings with Mg^{2+} and Cr^{6+} (Appendix Table 10 and Fig. 11a). This factor is indicative of geogenic processes, such as gypsum, halite, anhydrite,

and dolomite dissolutions, as well as ion exchange and weathering of minerals from the bearing layers. Factor 2 accounts for 20.71% of the total variance and has an eigenvalue of 4.24 (Appendix Table 10). It exhibits strong loadings with pH, K^+ , Fe^{2+} , and Zn^{2+} (Appendix Table 10 and Fig. 11a). Alkaline water dominated the study area, and the weathering of clay minerals serves as the primary source of K^+ in groundwater. On the other hand, Factor 3 represents 16.25% of the total variance and has an eigenvalue of 3.34 (Appendix Table 10). It shows strong loadings with Tem, Ca^{2+} , and Al^{3+} (Appendix Table 10 and Fig. 11a). This factor is associated with gypsum and calcite dissolution. Factor 4 explains 14.71% of the total variance and has an eigenvalue of 2.77 (Appendix Table 10). It shows strong loadings with Ba^{2+} , Cu^+ , and Mn^{2+} (Appendix Table 10 and Fig. 11b), indicating weathering of the bearing layers containing these minerals, likely due to geogenic processes. Anthropogenic influences are absent in this factor. On the other hand, Factor 5 accounts for 9.07% of the total variance and has an eigenvalue of 1.64 (Appendix Table 10). It exhibits moderate loadings with NO_3^- and HCO_3^- (Appendix Table 10 and Fig. 11b). This factor suggests a recharge area from the Nile River and Rainfall.

3.4.6 Cluster Analysis

In the first zone, we applied the ward linkage method using z-standardized input data from 68 samples and 23 parameters (Fig. 12a). This analysis resulted in the identification of five major clusters. Cluster 1 comprises 12 groundwater samples, with TDS values ranging from 980 to 3370 mg L^{-1} , an average of 2019 mg L^{-1} , and a standard deviation of 579 (Table 1). The water types within this cluster are characterized by $\text{Na}^+\text{-Cl}^-$ and $\text{Na}^+\text{-SO}_4^{2-}$. These patterns suggest the influence of geogenic processes, particularly halite and gypsum dissolution. Various mineral saturation indices were analyzed for all clusters. For all five clusters, the water was oversaturated for calcite and dolomite, and undersaturated for anhydrite, gypsum, and halite (Appendix Table 11). In contrast, Cluster 2 consists of 7 groundwater samples (Fig. 9a), with TDS values ranging from 786 to 1260 mg L^{-1} , a mean of 987 mg L^{-1} , and a standard deviation of 190 (Table 1). The water types in this cluster are solely associated with $\text{Na}^+\text{-Cl}^-$. This indicates a discharge area with a notable presence of halite dissolution. Cluster 3 comprises 9 groundwater samples (Fig. 12a),

with TDS values ranging from 431 to 1210 mg L⁻¹, an average of 742 mg L⁻¹, and a standard deviation of 247 (Table 1). The water types within this cluster include Na⁺-Cl⁻, Na⁺-Ca²⁺-SO₄²⁻ and Na⁺-HCO₃⁻, indicating a connection to meteoric recharge and halite/gypsum dissolution processes. On the other hand, Cluster 4 includes 12 groundwater samples (Fig. 12a), with TDS values ranging from 263 to 679 mg L⁻¹, an average of 475 mg L⁻¹, and a standard deviation of 128 (Table 1). This cluster is characterized by low TDS values. The water types associated with this cluster are Na⁺-HCO₃⁻ and Na⁺-Cl⁻-HCO₃⁻, with only one sample showing a relation to Na⁺-Cl⁻ type. These findings suggest a direct recharge area from the Nile River and rainfall. The five clusters encompass 27 groundwater samples (Fig. 12a). TDS values in these samples range from 270 to 1166 mg L⁻¹, with a mean of 710 mg L⁻¹ and a standard deviation of 260 (Table 1). The predominant water types are Na⁺-Cl⁻, with three samples showing Na⁺-HCO₃⁻ characteristics. Halite dissolution appears to be the dominant process influencing the water composition.

In the second zone, we analyzed twenty-five samples with 23 parameters. The Furthest Neighbor method was applied, resulting in the identification of three major clusters. The first cluster comprises 4 groundwater samples (Fig. 12b) with TDS values ranging from 688 to 855 mg L⁻¹, an average of 737 mg L⁻¹, and a standard deviation of 79.52 (Table 2). This cluster displays two water types, specifically mixed types with Na⁺-Mg²⁺-Ca²⁺-Cl⁻-HCO₃⁻ and Na⁺-Ca²⁺-Mg²⁺-Cl⁻-HCO₃⁻ compositions. These patterns indicate ion exchange between Na⁺, Ca²⁺, and Mg²⁺, along with dolomite, calcite, and halite dissolutions. The saturation values indicated that calcite and dolomite were in the upper saturation state, while gypsum and halite were in the undersaturation state (Appendix Table 12). The second cluster comprises 6 groundwater samples (Fig. 12b). TDS values in this cluster range from 709 to 912 mg L⁻¹, with an average of 816.5 mg L⁻¹ and a standard deviation of 88.41 (Table 2). This cluster exhibits two water types: Na⁺-Mg²⁺-Ca²⁺-Cl⁻-HCO₃⁻ and Na⁺-Mg²⁺-Cl⁻-HCO₃⁻. The dominant elements in these samples are Na⁺, Mg²⁺, Cl⁻, and HCO₃⁻. This cluster is indicative of a mixture of saline water and fresh recharge water from the Nile River and rainfall. The saturation index (SI) values also indicated upper saturation for calcite and dolomite, and

undersaturation for gypsum and halite (Appendix Table 12). The third cluster comprises 14 groundwater samples (Fig. 12b). TDS values in this cluster range from 645 to 810 mg L⁻¹, with a mean of 715.9 mg L⁻¹ and a standard deviation of 45.11 (Table 2). The groundwater types observed in this cluster include Na⁺-Ca²⁺-Mg²⁺-Cl⁻-HCO₃⁻, Na⁺-Mg²⁺-Ca²⁺-Cl⁻-HCO₃⁻, Na⁺-Mg²⁺-Cl⁻-HCO₃⁻, and Na⁺-Ca²⁺-Cl⁻-HCO₃⁻. These patterns are indicative of gypsum, halite, calcite, and dolomite dissolutions, as well as rock-water interactions involving ion exchange processes. Moreover, the cluster suggests a mixing of recharge sources, including water from the Nile River and rainfall. The saturation index values showed undersaturation for gypsum and halite, and upper saturation for calcite and dolomite (Appendix Table 12).

In the third zone, we utilized eleven samples with 23 parameters and the ward method to identify three major clusters. The first cluster, containing 3 samples (Fig. 12c), showed TDS values ranging from 1025 to 1242 mg L⁻¹, with a mean of 1136 mg L⁻¹ and a standard deviation of 108.6 (Table 3). The saturation values indicated oversaturation for calcite and dolomite and undersaturation for gypsum and halite (Appendix Table 13). This cluster displayed two water types, Na⁺-Ca²⁺-Cl⁻-SO₄²⁻ and Na⁺-Ca²⁺-Cl⁻-HCO₃⁻, suggesting a mixing of fresh and saline water from different sources, such as the Nile River and rainfall. Meanwhile, the second cluster comprised 2 samples (Fig. 12c), with TDS values ranging from 1893 to 1982 mg L⁻¹, an average of 1937, and a standard deviation of 62.93 (Table 3). The dominant water type in this cluster was Na⁺-Ca²⁺-Cl⁻, indicating halite and calcite dissolution. Saturation values indicated undersaturation for gypsum and halite, and upper saturation for calcite and dolomite (Appendix Table 13). On the other hand, the third cluster included 5 samples (Fig. 12c), showing TDS values ranging from 1663 to 1938 mg L⁻¹, with an average of 1780 mg L⁻¹ and a standard deviation of 100 (Table 3). This cluster exhibited three water types: Na⁺-Ca²⁺-Cl⁻, Na⁺-Cl⁻, and Na⁺-Mg²⁺-Cl⁻. Saturation values indicated upper saturation for calcite and dolomite, and undersaturation for gypsum and halite (Appendix Table 13). These patterns suggested high dissolution of halite, dolomite, and calcite, as well as ion exchange processes.

4 Conclusion

For this research, hydrochemical investigations, incorporating analyses of geochemistry, multivariate statistics, and geostatistics, were conducted to gain insights into the elements affecting groundwater geochemistry and the potential for pollution. A comprehensive analysis was performed on 104 groundwater samples, examining twenty-three physical, chemical, and trace variables for each sample. Based on the lineament map, cluster analysis, water types, and geologic map, the study area was divided into three main zones. The first zone has a high lineament density in its central part, the second zone exhibits a similar high density in its eastern part, while the third zone has high lineament density in the western and northern parts. Spatial variations in total dissolved solids (TDS) and nitrate concentration, influencing groundwater quality, were mapped. A clear spatial pattern in water table depth emerged, increasing from south to north in the study area. It is noticed that groundwater salinity increases northeastward, where the groundwater becomes deeper. Meanwhile, shallow groundwater with low salinity is recorded in the south and west areas, where the aquifer is recharged with fresh Nile water. The elevated TDS values were associated with geogenic processes, specifically water–rock interactions, where groundwater deeply percolated and dissolved aquifer minerals when it flows from the Red Sea hills to reach the Nile valley. This leads to higher ion concentrations in groundwater, such as the dissolution of evaporite and carbonate rocks, as well as ion exchange. Additionally, anthropogenic processes, such as irrigation return flow, contributed to the increased salinity levels in the groundwater, spatially in the irrigated area with groundwater. A significant correlation was observed between NO_3^- levels and agricultural activity. The first zone, near the Nile with small depths and flood irrigation, had higher NO_3^- levels. Moving north with increased depth and drip irrigation, NO_3^- levels decreased, indicating agriculture as the primary NO_3^- source in the groundwater in the first zone. The Piper diagram classification revealed three zones and six distinct groundwater types (facies) in the first zone, five types in the second zone, and five types in the third zone. These results imply the existence of particular hydrochemical processes, involving the dissolution of evaporite and carbonate rocks such as anhydrite, gypsum, halite, calcite, and dolomite, along with ion exchange. The predominant processes included

meteoric water recharge, where saline water from the Nile River and rainfall played a substantial role. In the drouve diagram classification, first-zone groundwater samples aligning with fields No. 2, 5, 6, and 9 signify meteoric groundwater recharge and the presence of dual sources marked by chemical imprints from the Nile river and rainfall precipitation. This conclusion finds reinforcement in ion exchange and substantial halite dissolution, corroborated by the saturation indices. Conversely, second and third zone samples uniformly falling into field No. 9 and tracing along the dissolution or mixing line indicate the amalgamation of groundwater from two or more distinct facies. This implies the existence of two diverse groundwater sources or mixed water, deriving from the Nile river and rainfall. Moreover, the impactful role of evaporite and carbonate rock dissolution, coupled with ion exchange, is evident in shaping the chemical composition of groundwater samples. The average saturation index values for minerals, including anhydrite, halite, and gypsum, were consistently negative, indicating prevalent under-saturation conditions. In contrast, the saturation index for dolomite and calcite indicated upper saturation conditions, implying the precipitation of secondary minerals. These findings offer valuable insights into the current chemical conditions of the groundwater. Additionally, through Gibbs diagram analysis and the relations between $\text{Ca}^{2+}/\text{Na}^+$ vs $\text{HCO}_3^-/\text{Na}^+$ and $\text{Ca}^{2+}/\text{Na}^+$ vs $\text{Mg}^{2+}/\text{Na}^+$, it became evident that rock-water interaction significantly dominates as the primary factor influencing groundwater chemistry. The correlation coefficients align with the saturation indices of aquifer minerals, serving as a tool to discern various processes influencing groundwater hydrochemistry, including the dissolution of aquifer minerals and ion exchange. Six factors were identified, describing more than 73.50%, 83.31%, and 89.88% of the total data variance for Zones 1, 2, and 3, respectively. These factors elucidate the chemical attributes of the groundwater, arising from interactions between rock and water, the blending of waters from diverse sources, and, to some extent, anthropogenic influences. Cluster analysis shows that there are five, three, and three significant clusters of samples for Zones 1, 2, and 3, respectively. This indicates that the original groundwater was uniquely influenced by different processes and recharge sources. These results could contribute to more effective water resource management at a regional level and may be applicable to numerous areas with comparable conditions.

Appendix

Table 5 Correlation matrix of physicochemical and trace constituents of groundwater samples in Zone 1

Parameters	O2	Eh	Temp	pH	EC	TDS	Ca	K	Mg	Na	F	Cl	NO3	SO4	HCO3	Al	Ba	Cr	Cu	Fe	Mn	Sr	Zn	
O2	1																							
Eh	0.01	1																						
Temp	0.00	-0.01	1																					
pH	-0.08	-0.58	0.09	1																				
EC	0.34	0.11	-0.35	-0.34	1																			
TDS	0.34	0.11	-0.35	-0.34	1.00	1																		
Ca	0.39	0.25	-0.23	-0.47	0.75	0.75	1																	
K	0.26	0.00	-0.09	-0.15	0.55	0.55	0.66	1																
Mg	0.14	-0.04	-0.26	-0.08	0.69	0.69	0.58	0.82	1															
Na	0.36	0.07	-0.34	-0.29	0.94	0.94	0.71	0.68	0.77	1														
F	0.49	0.05	0.02	-0.32	0.42	0.42	0.38	0.15	0.04	0.40	1													
Cl	0.31	0.03	-0.33	-0.23	0.88	0.88	0.63	0.73	0.86	0.97	0.27	1												
NO3	0.35	0.30	-0.26	-0.60	0.66	0.66	0.79	0.31	0.31	0.59	0.50	0.48	1											
SO4	0.38	0.16	-0.19	-0.37	0.75	0.75	0.93	0.62	0.51	0.70	0.46	0.57	0.73	1										
HCO3	-0.31	0.27	-0.18	-0.16	0.07	0.07	0.03	-0.06	-0.04	0.04	-0.11	-0.03	0.06	0.03	1									
Al	0.06	-0.27	-0.07	0.37	-0.04	-0.04	-0.06	0.08	0.08	-0.07	0.03	-0.04	-0.10	-0.02	-0.14	1								
Ba	0.07	0.15	-0.28	-0.05	0.01	0.01	0.05	0.03	0.04	0.07	-0.06	0.07	0.05	0.01	0.10	0.27	1							
Cr	0.22	0.15	-0.12	-0.21	0.18	0.18	0.22	0.23	0.21	0.19	0.00	0.21	0.12	0.19	-0.10	-0.04	0.16	1						
Cu	0.24	0.18	-0.06	-0.28	0.13	0.13	0.16	0.06	0.02	0.10	0.30	0.06	0.27	0.16	0.11	0.11	0.08	0.10	1					
Fe	0.15	-0.22	-0.06	0.21	0.04	0.04	0.14	0.15	0.11	0.04	0.15	0.03	0.00	0.16	-0.02	0.58	0.31	0.06	0.35	1				
Mn	-0.25	0.21	0.03	0.14	-0.06	-0.06	-0.12	-0.09	-0.08	-0.07	-0.16	-0.08	-0.10	-0.11	0.25	0.18	0.30	-0.23	0.11	0.18	1			
Sr	0.15	0.14	0.04	-0.06	0.02	0.02	0.04	-0.05	0.03	0.03	-0.01	0.03	0.11	0.02	-0.10	-0.24	-0.02	0.11	-0.13	-0.17	-0.21	1		
Zn	-0.15	-0.24	-0.13	0.48	-0.01	-0.01	-0.05	0.11	0.18	-0.05	-0.23	0.00	-0.23	-0.02	0.15	0.47	0.19	-0.22	0.09	0.49	0.47	-0.27	1	

Table 6 Correlation matrix of physicochemical and trace constituents of groundwater samples in Zone 2

Parameters	O2	Eh	Temp	pH	EC	TDS	Ca	K	Mg	Na	F	Cl	NO3	SO4	HCO3	Al	Ba	Cr	Cu	Fe	Mn	Sr	Zn	
O2	1																							
Eh	-0.37	1																						
Temp	-0.53	0.10	1																					
pH	0.28	-0.24	-0.56	1																				
EC	-0.27	0.03	0.52	-0.07	1																			
TDS	-0.27	0.03	0.52	-0.07	1.00	1																		
Ca	-0.21	-0.07	0.38	0.08	0.76	0.76	1																	
K	0.16	-0.15	0.00	0.13	0.43	0.43	0.53	1																
Mg	-0.36	0.16	0.50	-0.19	0.84	0.84	0.36	0.26	1															
Na	-0.21	-0.01	0.49	-0.06	0.98	0.98	0.74	0.42	0.83	1														
F	-0.36	0.00	0.75	-0.46	0.81	0.81	0.55	0.06	0.71	0.80	1													
Cl	-0.21	0.02	0.45	0.02	0.97	0.97	0.76	0.51	0.83	0.98	0.71	1												
NO3	-0.22	0.11	0.65	-0.66	0.61	0.61	0.33	0.07	0.55	0.61	0.88	0.49	1											
SO4	-0.21	-0.06	0.45	-0.02	0.95	0.95	0.74	0.29	0.80	0.96	0.83	0.91	0.59	1										
HCO3	0.35	-0.24	-0.58	0.33	-0.26	-0.26	-0.16	0.10	-0.29	-0.24	-0.47	-0.26	-0.46	-0.19	1									
Al	0.02	0.26	-0.31	0.23	0.10	0.10	0.16	0.19	0.02	0.13	-0.16	0.19	-0.13	0.07	0.09	1								
Ba	-0.01	0.25	-0.18	0.38	0.13	0.13	0.27	0.30	-0.04	0.08	-0.11	0.08	-0.05	0.12	0.26	0.34	1							
Cr	-0.34	-0.10	0.31	-0.29	0.28	0.28	0.41	0.09	0.12	0.25	0.39	0.22	0.26	0.30	0.03	0.31	0.00	1						
Cu	-0.24	0.04	0.36	0.01	0.49	0.49	0.64	0.18	0.22	0.47	0.40	0.46	0.31	0.46	-0.17	-0.11	0.21	-0.08	1					
Fe	-0.17	-0.07	-0.12	0.17	0.09	0.09	0.31	0.17	0.01	0.06	-0.04	0.10	-0.21	0.14	0.22	0.51	0.22	0.67	-0.21	1				
Mn	0.16	-0.17	-0.21	0.22	-0.14	-0.14	0.07	0.33	-0.26	-0.15	-0.18	-0.13	-0.18	-0.15	0.12	-0.04	0.11	-0.13	0.13	-0.07	1			
Sr	-0.37	-0.05	0.34	-0.43	0.19	0.19	0.29	-0.11	0.02	0.17	0.42	0.10	0.35	0.21	-0.05	0.21	-0.11	0.91	-0.08	0.44	-0.17	1		
Zn	0.00	-0.19	-0.26	0.22	-0.11	-0.11	0.18	0.35	-0.25	-0.10	-0.23	-0.04	-0.29	-0.17	0.11	0.36	-0.08	0.34	-0.10	0.24	0.61	0.28	1	

Table 7 Correlation matrix of physicochemical and trace constituents of groundwater samples in Zone 3

Parameters	O2	Eh	Temp	pH	EC	TDS	Ca	K	Mg	Na	F	Cl	NO3	SO4	HCO3	Al	Ba	Cr	Cu	Fe	Mn	Sr	Zn	
O2	1																							
Eh	0.09	1																						
Tem	-0.27	0.44	1																					
pH	0.10	-0.45	0.20	1																				
EC	0.61	0.09	0.29	0.47	1																			
TDS	0.61	0.09	0.29	0.47	1	1																		
Ca	-0.01	0.45	0.57	0.04	0.62	0.62	1																	
K	0.13	-0.41	0.32	0.91	0.66	0.66	0.27	1																
Mg	0.63	-0.43	-0.17	0.57	0.56	0.56	-0.29	0.58	1															
Na	0.69	0.16	0.27	0.42	0.99	0.99	0.58	0.59	0.57	1														
F	-0.44	0.30	0.33	-0.25	-0.11	-0.11	0.13	-0.13	-0.12	-0.14	1													
Cl	0.51	0.02	0.35	0.62	0.96	0.96	0.53	0.78	0.63	0.95	0.00	1												
NO3	0.31	0.10	-0.49	-0.17	-0.09	-0.09	-0.12	-0.25	-0.12	-0.06	-0.47	-0.22	1											
SO4	0.42	0.11	0.45	0.36	0.93	0.93	0.71	0.66	0.42	0.91	0.07	0.92	-0.25	1										
HCO3	0.06	0.23	-0.22	-0.53	-0.20	-0.20	0.10	-0.65	-0.46	-0.17	-0.38	-0.42	0.29	-0.34	1									
Al	-0.32	0.07	0.62	0.50	0.41	0.41	0.72	0.56	-0.22	0.34	-0.08	0.44	-0.33	0.48	-0.04	1								
Ba	0.22	0.06	0.03	0.30	0.34	0.34	0.25	0.24	0.10	0.35	-0.07	0.33	0.43	0.21	-0.01	0.15	1							
Cr	0.16	0.30	0.25	-0.04	0.56	0.56	0.67	0.24	0.02	0.53	0.17	0.52	-0.32	0.67	-0.10	0.40	-0.38	1						
Cu	0.15	0.37	0.41	0.17	0.52	0.52	0.69	0.27	-0.14	0.53	-0.02	0.48	0.20	0.52	0.05	0.50	0.81	0.05	1					
Fe	-0.12	-0.14	0.38	0.75	0.39	0.39	0.26	0.77	0.25	0.32	-0.14	0.50	-0.12	0.39	-0.51	0.62	-0.10	0.35	0.02	1				
Mn	0.00	0.27	0.16	0.02	0.32	0.32	0.62	0.06	-0.33	0.31	-0.10	0.22	0.37	0.27	0.34	0.46	0.80	-0.04	0.91	-0.11	1			
Sr	-0.20	0.49	0.17	-0.37	-0.45	-0.45	-0.13	-0.57	-0.45	-0.40	-0.02	-0.49	-0.14	-0.50	0.47	-0.04	-0.54	0.02	-0.41	-0.09	-0.34	1		
Zn	-0.31	-0.63	0.15	0.85	0.11	0.11	-0.09	0.80	0.31	0.03	-0.18	0.28	-0.17	0.13	-0.59	0.48	0.08	-0.13	-0.02	0.76	-0.09	-0.4	1	

Table 8 The factor loadings for each of the 23 variables. Values in yellow represent significant factor loadings in Zone 1

Parameters	1	2	3	4	5	6
O2	0.252	0.084	0.508	-0.516	0.192	-0.011
Eh	0.035	-0.366	0.333	0.574	0.397	-0.103
Tem	-0.269	-0.052	0.028	-0.091	-0.073	-0.839
pH	-0.227	0.507	-0.550	-0.304	-0.251	0.003
EC	0.893	-0.064	0.253	0.001	-0.068	0.224
TDS	0.893	-0.064	0.253	0.001	-0.068	0.224
Ca	0.785	-0.055	0.425	0.048	0.129	-0.026
K	0.828	0.155	-0.059	-0.051	0.196	-0.277
Mg	0.893	0.129	-0.218	-0.031	0.141	-0.032
Na	0.929	-0.050	0.159	-0.047	0.001	0.182
F	0.237	-0.015	0.753	-0.274	-0.222	0.018
Cl	0.932	-0.015	0.004	-0.072	0.056	0.149
NO3	0.536	-0.210	0.641	0.066	0.022	0.179
SO4	0.750	-0.006	0.451	-0.005	0.022	-0.033
HCO3	0.024	-0.072	0.014	0.699	-0.118	0.223
Al	-0.036	0.793	0.030	-0.137	0.025	0.085
Ba	-0.036	0.372	0.069	0.225	0.527	0.440
Cr	0.187	-0.080	0.028	-0.182	0.757	0.012
Cu	0.007	0.285	0.616	0.182	0.127	-0.069
Fe	0.042	0.809	0.245	-0.053	0.136	0.007
Mn	-0.069	0.402	-0.045	0.664	-0.068	-0.049
Sr	-0.010	-0.380	-0.038	-0.250	0.323	0.083
Zn	0.088	0.760	-0.256	0.274	-0.173	0.031
Eigenvalues	7.482	3.018	2.094	1.911	1.355	1.045
% of Variance	28.567	12.607	11.970	8.672	6.256	5.430
Cumulative %	28.567	41.174	53.144	61.816	68.071	73.501

Extraction Method: Principal Component Analysis. Rotation Method: Varimax with Kaiser Normalization.a. Rotation converged in 11 iterations

Table 9 The factor loadings for each of the 23 variables. Values in yellow represent significant factor loadings in Zone 2

Parameters	1	2	3	4	5	6
O2	-0.103	0.481	-0.305	0.078	-0.443	-0.298
Eh	-0.043	-0.175	-0.106	-0.157	0.874	0.074
Tem	0.401	-0.745	0.102	-0.138	0.001	0.240
pH	0.017	0.801	-0.163	0.168	-0.017	0.129
EC	0.968	-0.127	0.089	-0.008	0.040	0.153
TDS	0.968	-0.127	0.089	-0.008	0.040	0.153
Ca	0.695	0.012	0.297	0.265	-0.031	0.482
K	0.497	0.272	-0.013	0.556	-0.017	0.049
Mg	0.854	-0.214	-0.069	-0.172	0.178	-0.153
Na	0.979	-0.107	0.065	-0.003	0.004	0.089
F	0.727	-0.576	0.173	-0.146	-0.108	0.132
Cl	0.979	-0.042	0.038	0.078	0.074	0.056
NO3	0.543	-0.636	0.056	-0.157	-0.031	0.074
SO4	0.937	-0.074	0.135	-0.104	-0.071	0.161
HCO3	-0.214	0.667	0.176	-0.073	-0.303	0.050
Al	0.151	0.421	0.414	0.194	0.559	-0.212
Ba	0.100	0.513	0.074	-0.040	0.368	0.559
Cr	0.181	-0.179	0.945	0.067	-0.041	-0.004
Cu	0.395	-0.150	-0.181	0.112	-0.024	0.758
Fe	0.087	0.363	0.782	0.022	0.133	-0.044
Mn	-0.151	0.063	-0.163	0.822	-0.128	0.202
Sr	0.055	-0.367	0.882	0.000	-0.067	0.001
Zn	-0.117	0.095	0.339	0.868	0.008	-0.136
Eigenvalues	8.599	3.428	2.819	1.766	1.463	1.086
% of Variance	32.335	15.588	12.920	8.872	6.955	6.645
Cumulative %	32.335	47.922	60.824	69.714	76.669	83.314

Extraction Method: Principal Component Analysis. Rotation Method: Varimax with Kaiser Normalization.a. Rotation converged in 11 iterations

Table 10 The factor loadings for each of the 23 variables. Values in yellow represent significant factor loadings in Zone 3

Parameters	1	2	3	4	5
O2	0.76	-0.19	-0.45	0.04	0.36
Eh	0.15	-0.68	0.46	0.07	-0.09
Tem	0.17	0.10	0.73	0.03	-0.39
pH	0.30	0.89	0.05	0.11	0.05
EC	0.95	0.17	0.17	0.19	0.02
TDS	0.95	0.17	0.17	0.19	0.02
Ca	0.48	-0.14	0.77	0.30	-0.05
K	0.50	0.84	0.13	0.11	-0.12
Mg	0.62	0.42	-0.58	-0.12	-0.09
Na	0.96	0.09	0.12	0.20	0.04
F	-0.09	-0.23	0.11	0.00	-0.92
Cl	0.90	0.34	0.14	0.16	-0.14
NO3	-0.10	-0.17	-0.29	0.44	0.59
SO4	0.88	0.16	0.29	0.15	-0.21
HCO3	-0.20	-0.59	0.16	0.06	0.62
Al	0.17	0.42	0.85	0.16	0.06
Ba	0.16	0.09	-0.07	0.95	0.06
Cr	0.63	-0.14	0.47	-0.38	-0.11
Cu	0.33	-0.05	0.40	0.83	0.00
Fe	0.25	0.74	0.41	-0.21	0.06
Mn	0.10	-0.14	0.38	0.87	0.20
Sr	-0.35	-0.41	0.33	-0.57	0.23
Zn	-0.08	0.99	0.09	0.03	-0.04
Eigenvalues	8.69	4.24	3.34	2.77	1.64
% of Variance	29.14	20.71	16.25	14.71	9.07
Cumulative %	29.14	49.85	66.10	80.81	89.88

Extraction Method: Principal Component Analysis. Rotation Method: Varimax with Kaiser Normalization.a. Rotation converged in 11 iterations

Table 11 Average cluster saturation indices (SI) values of the different mineral phases in Zone 1

Parameters	Anhydrite	Halite	Gypsum	Dolomite	Calcite
Clustal I	-1.38	-4.88	-1.10	2.22	1.14
Clustal II	-1.79	-5.59	-1.52	2.78	1.32
Clustal III	-1.83	-6.00	-1.55	2.09	1.06
Clustal IV	-2.30	-6.53	-2.03	2.06	1.02
Clustal V	-2.07	-5.98	-1.80	2.36	1.14

Table 12 Average cluster saturation indices (SI) values of the different mineral phases in Zone 2

Parameters	Anhydrite	Halite	Gypsum	Dolomite	Calcite
Clustal I	-2.02	-5.90	-1.77	2.12	0.99
Clustal II	-2.03	-5.75	-1.77	2.54	1.18
Clustal III	-2.0543	-5.8829	-1.7964	2.5529	1.1900

Table 13 Average cluster saturation indices (SI) values of the different mineral phases in Zone 3

Parameters	Anhydrite	Halite	Gypsum	Dolomite	Calcite
Clustral I	-1.61	-5.50	-1.34	0.97	0.49
Clustral II	-1.33	-5	-1.08	1.71	0.95
Clustral III	-1.51	-5.05	-1.25	1.53	0.69

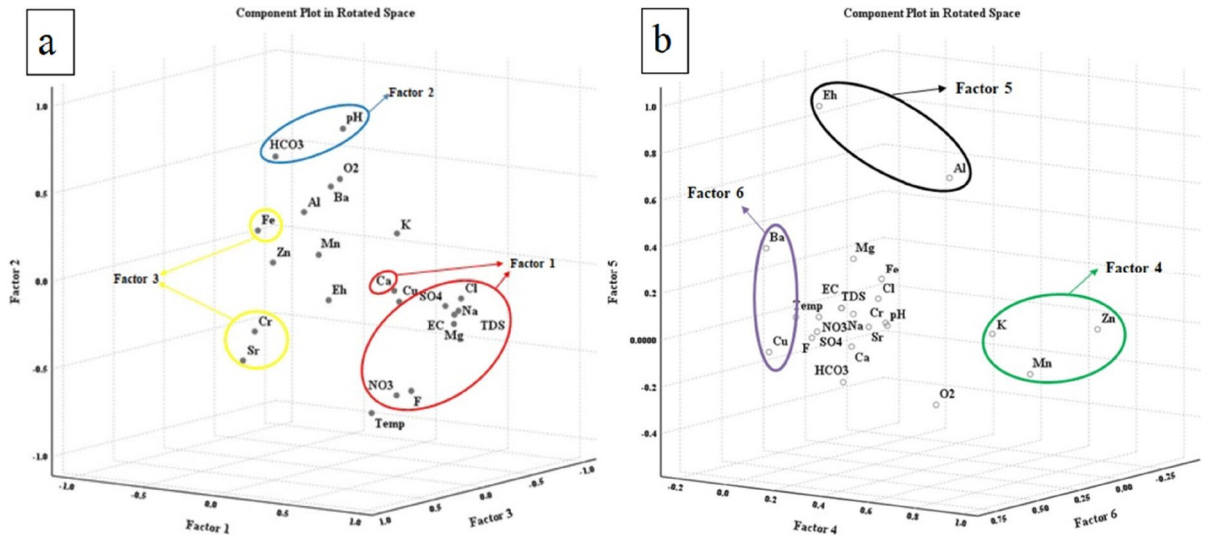


Fig. 13 Lineament density map for three zones

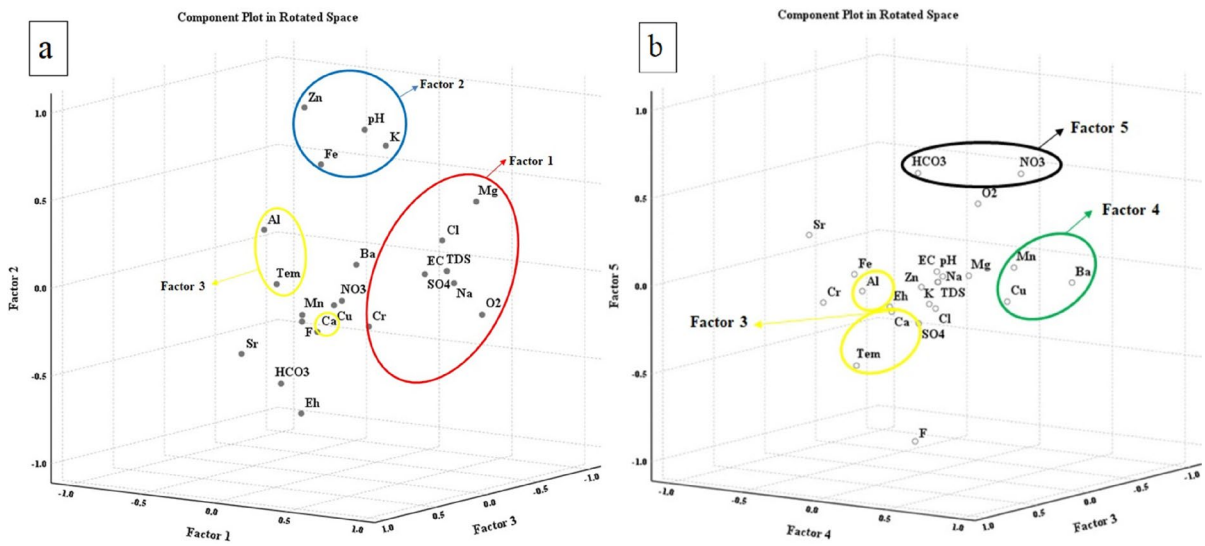


Fig. 14 Irrigated zones in the study area

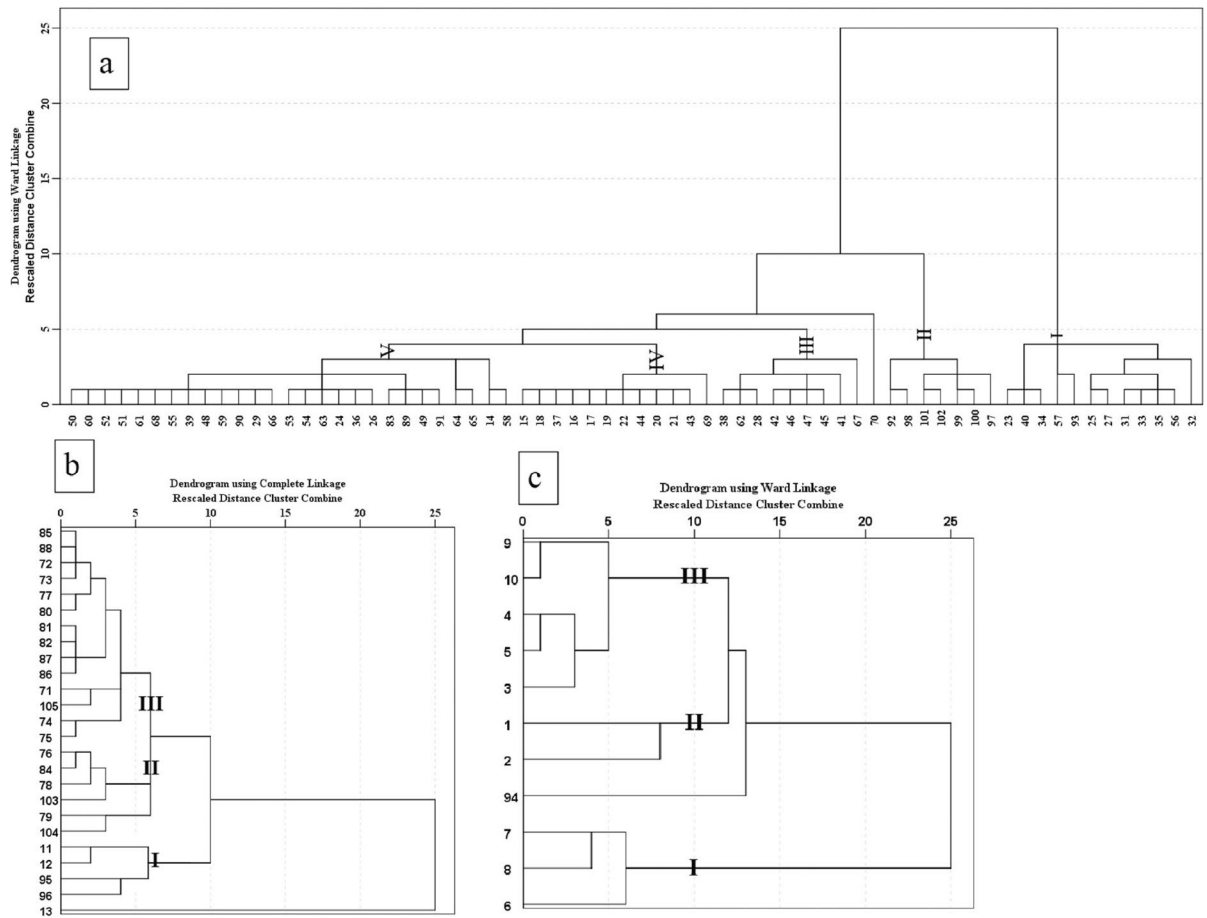


Fig. 15 Plot of HCO_3/Na vs Ca/Na and Mg/Na vs Ca/Na for three zones (Mthembu et al., 2020)

Acknowledgements The authors would like to thank the Geology Department of Mansoura University for logistical support, and express their gratitude to the editor, associate editor, and reviewers for their valuable comments.

Funding This research received no external funding.

Data Availability The datasets used and/or analyzed during the current study are available from the corresponding author on reasonable request.

Declarations

Conflicts of Interest The authors declare no conflict of interest.

References

- AbdEllah, R. G. (2020). Water resources in Egypt and their challenges, Lake Nasser case study. *The Egyptian Journal of Aquatic Research*, 46(1), 1–2.
- Abdel Moneim, A. A. (2005). Overview of the geomorphological and hydrogeological characteristics of the Eastern Desert of Egypt. *Hydrogeology Journal*, 13(2), 416–425. <https://doi.org/10.1007/S10040-004-0364-Y>
- Al-Bassam, A. M., & Khalil, A. R. (2012). DurovPwin: a new version to plot the expanded Durov diagram for hydrochemical data analysis. *Computers & Geosciences*, 42, 1–6. <https://www.sciencedirect.com/science/article/pii/S0098300412000404>. Accessed 27 February 2023

- El Alfy, M., Alharbi, T., & Mansour, B. (2018). Integrating geochemical investigations and geospatial assessment to understand the evolutionary process of hydrochemistry and groundwater quality in arid areas. *Environmental Monitoring and Assessment*, 190, 1–18. https://scholar.google.com/citations?view_op=view_citation&hl=en&user=gn7bq5IAAAAJ&sortby=pubdate&citation_for_view=gn7bq5IAAAAJ:Zph67rFs4hoC. Accessed 31 July 2024
- Alther, G. A. (1979). A Simplified Statistical Sequence Applied to Routine Water Quality Analysis: A Case History. *Groundwater*, 17(6), 556–561. <https://doi.org/10.1111/J.1745-6584.1979.TB03356.X>
- Amer, R., Ripperdan, R., Wang, T., & Encarnación, J. (2012). Groundwater quality and management in arid and semi-arid regions: case study, Central Eastern Desert of Egypt. *Journal of African Earth Sciences*, 69, 13–25. <https://www.sciencedirect.com/science/article/pii/S1464343X12000696>. Accessed 25 February 2023
- Ammar, A. I., & Kamal, K. A. (2018). Resistivity method contribution in determining of fault zone and hydro-geophysical characteristics of carbonate aquifer, eastern desert Egypt. *Applied Water Science*, 8(1), 1–27. <https://doi.org/10.1007/S13201-017-0639-9>
- Ayyad, S., & Khalifa, M. (2021). Will the Eastern Nile countries be able to sustain their crop production by 2050? An outlook from water and land perspectives. *Science of the Total Environment*, 775, 145769.
- Bagheri, R., Nosrati, A., Jafari, H., Eggenkamp, H. G. M., & Mozafari, M. (2019). Overexploitation hazards and salinization risks in crucial declining aquifers, chemo-isotopic approaches. *Journal of Hazardous Materials*, 369, 150–163.
- Bishay, Y. (1961). Biostratigraphic study of the Eocene in the Eastern Desert between Samalut and Assiut by the large foraminifera. https://scholar.google.com/scholar?hl=en&as_sdt=0%2C5&q=bishay+1961+samalut&btnG=&oq=bishay+1961+sa. Accessed 26 February 2023
- Bishay, Y. (1966). Studies on the larger Foraminifera of the Eocene of the Nile Valley between Assiut, Cairo and S.W. Sinai. *Ph. D. Thesis, Alexandria Univ.* Accessed 26 February 2023
- Davis, J. C., & Sampson, R. J. (2002). *Statistics and Data Analysis in Geology* (Vol. 646). New York: Wiley.
- Deutsch, W. J. (2020). *Groundwater geochemistry: fundamentals and applications to contamination*. CRC Press.
- Domenico, P. A., & Schwartz, F. W. (1997). Physical and chemical hydrogeology. *John Wiley and Sons*.
- Egyptian Metrological Authority. (1996). Climatic atlas of Egypt. *Published, Arab Republic of Egypt, Ministry of Transport*.
- El Alfy, M. (2013). Hydrochemical Modeling and Assessment of Groundwater Contamination in Northwest Sinai Egypt. *Water Environment Research*, 85(3), 211–223. <https://doi.org/10.2175/106143012X1356205145055>
- El Alfy, M., Abdalla, F., Moubark, K., & Alharbi, T. (2019). Hydrochemical equilibrium and statistical approaches as effective tools for identifying groundwater evolution and pollution sources in arid areas. *Geoscience Journal*, 23(2), 299–314.
- El Alfy, M., Lashin, A., Abdalla, F., & Al-Bassam, A. (2017). Assessing the hydrogeochemical processes affecting groundwater pollution in arid areas using an integration of geochemical equilibrium and multivariate statistical techniques. *Environmental Pollution*, 229, 760–770.
- El Alfy, M. O. H. A. M. E. D., & Merkel, B. (2006). Hydrochemical relationships and geochemical modeling of ground water in Al Arish area, North Sinai Egypt. *Hydrological Science and Technology*, 22(1–4), 47.
- El Amrawy, M. A., Hewaidy, A. G. A., Moussa, B. M., Abdel Hafz, N. A., El Abd, E. S. A., & Abu Risha, U. A. (2020). Hydrogeologic investigations to determine the sources of groundwater recharge of Samalut carbonate aquifer in some wadis, East El Minia Egypt. *NRIAG Journal of Astronomy and Geophysics*, 9(1), 206–219.
- El-Alfy, M., & Abdalla, F. (2019). *Water Resources in Egypt* (Vol. 1). Accessed 23 March 2023
- El-Alfy, M., Alharbi, T., & Mansour, B. (2018). Integrating geochemical investigations and geospatial assessment to understand the evolutionary process of hydrochemistry and groundwater quality in arid areas. *Environmental Monitoring and Assessment*, 190(5), 1–18. <https://doi.org/10.1007/S10661-018-6640-4>
- El-Saadawy, O., Gaber, A., Othman, A., Abotalib, A. Z., El Bastawesy, M., & Attwa, M. (2020). Modeling Flash Floods and Induced Recharge into Alluvial Aquifers Using Multi-Temporal Remote Sensing and Electrical Resistivity Imaging. *Sustainability*, 12(23), 10204.
- Elshaeb, M. A., El-Badawy, S. M., & Shaway, E. S. A. (2014). Development and impact of the Egyptian climatic conditions on flexible pavement performance. *American Journal of Civil Engineering and Architecture*, 2(3), 115–121. <https://doi.org/10.12691/ajcea-2-3-4>
- Embaby, A., Razack, M., Lecoz, M., & Porel, G. (2016). Hydrogeochemical Assessment of Groundwater in the Precambrian Rocks, South Eastern Desert Egypt. *Journal of Water Resource and Protection*, 8(03), 293–310. <https://doi.org/10.4236/jwarp.2016.83025>
- Freeze, R. A., & Cherry, A. J. (1979). *Groundwater*, Prentice Hall. *Inc. New Jersey*. https://scholar.google.com/scholar?hl=en&as_sdt=0%2C5&q=Freeze%2C+R.+and+Cherry%2C+A.+%281979%29%3A+Ground+water.+Prentice-Hall%2C+Upper+Saddle+River%2C+New+Jersey%2C+604+p.&btnG=. Accessed 27 February 2023
- Furi, W., Razack, M., Abiye, T. A., Kebede, S., & Legesse, D. (2012). Hydrochemical characterization of complex volcanic aquifers in a continental rifted zone: the Middle Awash basin. *Ethiopia. Hydrogeology Journal*, 2(20), 385–400.
- Gad, M., & Saad, A. (2017). Hydrogeochemical evaluation of fractured Limestone aquifer by applying a geochemical model in eastern Nile Valley. *Egypt. Environmental Earth Sciences*, 76(18), 1–11. <https://doi.org/10.1007/S12665-017-6974-1>
- Gemal, K., Ibrahim, A., & Bedair, S. (2021). Geophysical Groundwater Exploration in Arid Regions Using Integrated Land-Based Magnetic and DC Resistivity Measurements: A Case Study at Gilf Kebir Area, South Western Desert, Egypt. *Groundwater in Egypt's deserts*, 105–129. https://doi.org/10.1007/978-3-030-77622-0_5/FIGURES/14
- Gemal, K. S., Attwa, M., Eleraki, M., & Zamzam, S. (2017). Imaging of wastewater percolation in heterogeneous soil using electrical resistivity tomography (ERT): A case study at east of Tenth of Ramadan City. *Egypt. Environmental*

- Earth Sciences*, 76(19), 1–17. <https://doi.org/10.1007/S12665-017-7013-Y/METRICS>
- Gemail, K. S., Ghoneimi, A., Shebl, S., Soliman, S., El-Sayed, K., & Saleh, A. H. (2024). Flow Pathways in Fractured Basalt under Challenging Environmental Conditions: A Synergistic Approach of Electrical Resistivity Tomography and Seismic Refraction Imaging. *Environmental Processes*, 11(2), 24. <https://doi.org/10.1007/S40710-024-00700-Y>
- Gulgundi, M. S., & Shetty, A. (2018). Groundwater quality assessment of urban Bengaluru using multivariate statistical techniques. *Applied Water Science*, 8(1), 1–15. <https://doi.org/10.1007/S13201-018-0684-Z>
- Habibah, A. A., Dahab, K., Shabana, A., Kamh, S., & Ibrahim, H. (2022). Assessment of the Hydrogeochemical Characteristics of Groundwater Resources at some Wadis in the East of El Minia Governorate, Eastern Desert Egypt. *Acta Geologica Sinica-English Edition*, 96(3), 1082–1097. <https://doi.org/10.1111/1755-6724.14654>
- Harmsen, J. (2016, January). A new and scalable approach for rural sanitation in Egypt: The Deir Gabal El-Tair pilot. In *The Environmental Technology for Impact conference (ETEI2015)*.
- Honarbaksh, A., Azma, A., Nikseresht, F., Mousazadeh, M., Eftekhari, M., & Ostovari, Y. (2019). Hydro-chemical assessment and GIS-mapping of groundwater quality parameters in semi-arid regions. *Journal of Water Supply: Research and Technology - AQUA*, 68(7), 509–522. <https://doi.org/10.2166/aqua.2019.009>
- Hussien, H. M. (2023). Hydrogeological and remote sensing investigation of the fractured carbonate aquifer, East El Minia, Eastern Desert Egypt. *Groundwater for Sustainable Development*, 23, 101006. <https://doi.org/10.1016/j.gsd.2023.101006>
- Ibrahim, A., Gemail, K. S., Bedair, S., Saada, S. A., Koch, M., & Nosair, A. (2023). An Integrated Approach to Unravel the Structural Controls on Groundwater Potentialities in Hyper-arid Regions Using Satellite and Land-Based Geophysics: A Case Study in Southwestern Desert of Egypt. *Surveys in Geophysics*, 44(3), 783–819. <https://doi.org/10.1007/S10712-022-09755-8>
- Islam, K. I. (2023). Predicting areal extent of groundwater contamination through geostatistical methods exploration in a data-limited rural basin. *Groundwater for Sustainable Development*, 23, 101043.
- Kaiser, H. F. (1958). The varimax criterion for analytic rotation in factor analysis. *Psychometrika*, 23(3), 187–200.
- Karroum, M., Elgettafi, M., Elmandour, A., Wilske, C., Himi, M., & Casas, A. (2017). Geochemical processes controlling groundwater quality under semi arid environment: A case study in central Morocco. *Science of the Total Environment*, 609, 1140–1151. <https://doi.org/10.1016/j.scitotenv.2017.07.199>
- Khalil, M. M., Abotalib, A. Z., Farag, M. H., Rabei, M., Abdelhady, A. A., & Pichler, T. (2021). Poor drainage-induced waterlogging in Saharan groundwater-irrigated lands: Integration of geospatial, geophysical, and hydrogeological techniques. *Catena*, 207, 105615.
- Kim, J. O., & Mueller, C. W. (1978). *Factor analysis: Statistical methods and practical issues* (Vol. 14). Sage.
- Kumar, V., Maity, A., Kumar, A., Saha, S., Kay, P., Singh, B., & Mukherjee, T. (2023). Critical review on uranium and arsenic content and their chemical mobilization in groundwater: A case study of the Malwa region Punjab India. *Science of The Total Environment*, 885, 163885.
- Li, M., Liang, X., Xiao, C., Cao, Y., & Hu, S. (2019). Hydrochemical evolution of groundwater in a typical semi-arid groundwater storage basin using a zoning model. *Water*, 11(7), 1334. <https://www.mdpi.com/487860>. Accessed 23 March 2023
- Lloyd, J., & Heathcote, J. (1985). Natural inorganic hydrochemistry in relation to ground water. <https://www.osti.gov/biblio/6026514>. Accessed 1 February 2023
- Loni, O. A., Zaidi, F. K., Alhumimidi, M. S., Alharbi, O. A., Hussein, M. T., Dafalla, M., et al. (2015). Evaluation of groundwater quality in an evaporation dominant arid environment; a case study from Al Asyah area in Saudi Arabia. *Arabian Journal of Geosciences*, 8(8), 6237–6247. <https://doi.org/10.1007/S12517-014-1623-4>
- Machiwal, D., Jha, M. K., Singh, V. P., & Mohan, C. (2018). Assessment and mapping of groundwater vulnerability to pollution: Current status and challenges. *Earth-Science Reviews*, 185, 901–927. <https://doi.org/10.1016/J.EARSCIREV.2018.08.009>
- Mahmoud, S. H. (2014). Investigation of rainfall–runoff modeling for Egypt by using remote sensing and GIS integration. *Catena*, 120, 111–121.
- Mthembu, P. P., Elumalai, V., Brindha, K., & Li, P. (2020). Hydrogeochemical Processes and Trace Metal Contamination in Groundwater: Impact on Human Health in the Maputaland Coastal Aquifer. *South Africa. Exposure and Health*, 12(3), 403–426. <https://doi.org/10.1007/s12403-020-00369-2>
- Musaed, H. A. H., Al-Bassam, A. M., Zaidi, F. K., Alfaifi, H. J., & Ibrahim, E. (2020). Hydrochemical assessment of groundwater in mesozoic sedimentary aquifers in an arid region: A case study from Wadi Nisah in Central Saudi Arabia. *Environmental Earth Sciences*, 79(6), 1–12. <https://doi.org/10.1007/S12665-020-8889-5>
- Musaed, H., El-Kenawy, A., & El Alfy, M. (2022). Morphometric, Meteorological, and Hydrologic Characteristics Integration for Rainwater Harvesting Potential Assessment in Southeast Beni Suef (Egypt). *Sustainability*, 14(21), 14183.
- Nan, Z., Bo, L., & Changlai, X. (2016). Spatio-temporal variation of groundwater contamination using IEA-UEF in urban areas of Jilin City, North-eastern China. *Water Science and Technology: Water Supply*, 16(5), 1277–1286.
- Narany, T., Sefie, A., & Aris, A. Z. (2018). The long-term impacts of anthropogenic and natural processes on groundwater deterioration in a multilayered aquifer. *Science of the total environment*, 630, 931–942. <https://www.sciencedirect.com/science/article/pii/S0048969718305898>. Accessed 1 February 2023
- Parkhurst, D. L., & Appelo, C. A. J. (1999). User's guide to PHREEQC (Version 2): A computer program for speciation, batch-reaction, one-dimensional transport, and inverse geochemical calculations. *Water-resources investigations report*, 99(4259), 312. http://acamedia.info/sciences/J_G/references/PHREEQC_Manual.pdf. Accessed 28 February 2023

- Porsani, J. L., Elis, V. R., & Hiodo, F. Y. (2005). Geophysical investigations for the characterization of fractured rock aquifers in Itu, SE Brazil. *Journal of Applied Geophysics*, 57(2), 119–128.
- Ruelleu, S., Moreau, F., Bour, O., Gapais, D., & Martelet, G. (2010). Impact of gently dipping discontinuities on basement aquifer recharge: An example from Ploemeur (Brittany, France). *Journal of Applied Geophysics*, 70(2), 161–168.
- Sahoo, P. K., Ray, S. B., Kerketta, A., Behera, P., Neogi, G., & Sahoo, H. B. (2022). Geogenic enrichment of fluoride in groundwater of hard rock aquifer in fluorosis prevalent area of Balangir district, Odisha, India. *Groundwater for Sustainable Development*, 19, 100830. <https://doi.org/10.1016/J.GSD.2022.100830>
- Said, R. (1960). The geology of Egypt: balkema. Rotterdam, Brookfield. https://scholar.google.com/scholar?hl=en&as_sdt=0%2C5&q=Said+R+%281990%29+The+Geology+of+Egypt.+Balkema%2C+Amsterdam%2C+New+York%2C+734+p&btnG=. Accessed 26 February 2023
- Said, R. (1981). *The Geological Evolution of the River Nile* (pp. 151). Springer. [https://books.google.com/eg/books?hl=en&lr=&id=8OKPBAAAQBAJ&oi=fnd&pg=PA1&dq=Said,+R.+\(1981\).+The+Geological+Evolution+of+the+River+Nile.+New+York&ots=YRF2SqvR_6&sig=Mk2lul38mC9lh6uISeL59_ao0zc&redir_esc=y#v=onepage&q=Said%2C%20R.%20\(1981\).](https://books.google.com/eg/books?hl=en&lr=&id=8OKPBAAAQBAJ&oi=fnd&pg=PA1&dq=Said,+R.+(1981).+The+Geological+Evolution+of+the+River+Nile.+New+York&ots=YRF2SqvR_6&sig=Mk2lul38mC9lh6uISeL59_ao0zc&redir_esc=y#v=onepage&q=Said%2C%20R.%20(1981).) Accessed 27 February 2023.
- Sargazi, S., Mokhtari, M., Ehrampoush, M. H., Almodaresi, S. A., Sargazi, H., & Sarhadi, M. (2021). The application of geographical information system (GIS) approach for assessment of groundwater quality of Zahedan city, Sistan and Baluchestan Province. *Iran. Groundwater for Sustainable Development*, 12, 100509. <https://doi.org/10.1016/J.GSD.2020.100509>
- Suk, H., & Lee, K. K. (1999). Characterization of a ground water hydrochemical system through multivariate analysis: Clustering into ground water zones. *Groundwater*, 37(3), 358–366. <https://doi.org/10.1111/j.1745-6584.1999.tb01112.x>
- Sultan, M., Sturchio, N. C., Gheith, H., Abdel Hady, Y., & El Anbeawy, M. (2000). Chemical and isotopic constraints on the origin of Wadi El-Tarfa ground water, Eastern Desert. *Egypt. Ground Water*, 38(5), 743–751.
- Sultan, M., Yousef, A. F., Metwally, S. E., Becker, R., Milewski, A., Sauck, W., & Welton, B. (2011). Red Sea rifting controls on aquifer distribution: Constraints from geochemical, geophysical, and remote sensing data. *GSA Bulletin*, 123(5–6), 911–924. <https://doi.org/10.1130/B30146.1>
- Tawab, S. A. (1994). A geotechnical evaluation of Minia-Maghagha area. Upper Egypt. *Journal of King Abdulaziz University, Earth Sciences*, 7, 143–157.
- Wederni, K., Ben Alya, M., Missaoui, R., & Hamed, Y. (2023). Assessment of groundwater hydrogeochemical characteristics and salinization intrusion in coastal arid area (South Gabes, South-East Tunisia). *Journal of African Earth Sciences*, 200, 104875. <https://doi.org/10.1016/J.JAFREARSCI.2023.104875>
- Youssef, Y. M., Gemail, K. S., Atia, H. M., & Mahdy, M. (2024). Insight into land cover dynamics and water challenges under anthropogenic and climatic changes in the eastern Nile Delta: inference from remote sensing and GIS data. *Science of the Total Environment*, 913, 169690. <https://www.sciencedirect.com/science/article/pii/S0048969723083201>. Accessed 31 July 2024
- Zhai, Y., Jiang, Y., Cao, X., Leng, S., & Wang, J. (2022). Valuation of ecosystem damage induced by soil-groundwater pollution in an arid climate area: Framework, method and case study. *Environmental Research*, 211, 113013. <https://doi.org/10.1016/J.ENVRES.2022.113013>

Publisher's Note Springer Nature remains neutral with regard to jurisdictional claims in published maps and institutional affiliations.

Springer Nature or its licensor (e.g. a society or other partner) holds exclusive rights to this article under a publishing agreement with the author(s) or other rightsholder(s); author self-archiving of the accepted manuscript version of this article is solely governed by the terms of such publishing agreement and applicable law.